

Effect of Variable Inlet Guide Vanes on the Operating Characteristics of a Tilt Nacelle Inlet/Powered Fan Model

R.R. Woollett
Lewis Research Center
Cleveland, Ohio

and

H.C. Pontonides
Grumman Aerospace Corporation
Bethpage, New York

September 1987

(NASA-TM-88983) EFFECT OF VARIABLE INLET
GUIDE VANES ON THE OPERATING CHARACTERISTICS
OF A TILT NACELLE INLET/POWERED FAN MODEL
(NASA) 41 p Avail: NTIS HC A03/MF A01

N87-27628

Unclas

CSC 01A G3/02 0094202



EFFECT OF VARIABLE-INLET GUIDE VANES ON THE OPERATING CHARACTERISTICS
OF A TILT NACELLE-INLET POWERED FAN MODEL

R.R. Woollett
National Aeronautics and Space Administration
Lewis Research Center
Cleveland, Ohio 44135

and

H.C. Pontonides
Grumman Aerospace Corporation
Bethpage, New York 11714

SUMMARY

The effects of a variable-inlet guide vane (VIGV) assembly on the operating characteristics of a V/STOL inlet and on the performance of a 20-in.- (0.508-m-) diameter fan engine were investigated. The data indicate that the VIGV's are effective thrust modulators over a wide range of free-stream velocities, nacelle angles-of-attack, and fan speeds. The thrust modulation ranges including choking limits, fan stall limits, and inlet separation boundaries are presented.

The presence of the VIGV assembly causes significant losses in inlet angle-of-attack capability and generally increases the blade stress levels at all limit conditions except at high angle-of-attack and high free-stream velocity.

Reducing the fan nozzle exit area limited the positive VIGV actuation range and consequently decreased the range of thrust modulation at all limit conditions except at both high free-stream velocity and high angle-of-attack conditions.

INTRODUCTION

Vertical lift aircraft require some method of thrust modulation to provide stability and control during takeoff, landing, and transitional flight. Two promising methods are the use of (1) variable-pitch fan rotor blades (VP) and (2) variable-inlet guide vanes (VIGV). Performance data for comparison of the two methods, tested statically under identical conditions, are contained in references 1 and 2. The VIGV installation in a test cell, reported in reference 1, provided static thrust variations from 68 to 114 percent of the thrust obtained at the design angle setting. The variable-pitch fan installation in a test cell reported in reference 2 provided a total static thrust variation from 15 to 115 percent of the thrust obtained at the design setting. In each of these experiments, the fan air was captured by means of a bellmouth inlet without a diffuser, thereby resulting in uniform and steady flow at the fan face. However, in actual use of the VIGV and/or variable-pitch rotor fan, the inlet and flow conditions could be significantly different than those obtained with a bellmouth inlet. How possible nonuniform and/or nonsteady flow

at the fan face will affect the fan's performance is not known. A wide range of distorted flow could be tested, including many conditions that would never be encountered in actual use. Therefore, to reduce data and consider only flow conditions encountered with a V/STOL vehicle, an inlet was tested at simulated flight conditions in a wind tunnel for realistic flow fields. In this test the fan was evaluated at distortions that are encountered in free flight. The results of references 1 and 2 were obtained from 1.32 and 1.38 pressure ratio fans, respectively. Since the present test was conducted with a 1.2 pressure ratio fan, the thrust variation obtained in the present test cannot be compared directly with the referenced results. In order to extend VIGV research to representative VTOL transitional speeds and inlet inflow angles, modifications were made on existing models. The Hamilton Standard VIGV subassembly of reference 1 was mated to the NASA Lewis 20-in.- (0.508-m-) diameter fan (NASA Rotor 55) and to an existing inlet subassembly. Performance of this inlet-fan combination without the VIGV's has previously been tested in the NASA Lewis 9- by 15-ft (2.743- by 4.572-m) Low-Speed Wind Tunnel to forward speeds up to 125 kn (64.3 m/sec) and angles of attack up to 120°. Summary results have been reported in reference 3.¹ The specific objectives of the present investigation are (1) to obtain fan stage performance at transitional flight speeds and at high inlet-flow angles and (2) to determine the effects of the VIGV's on the fan aeromechanics and on the performance and angle-of-attack capability of an already documented inlet fan system.

SYMBOLS

A	area
D	diameter
EO	engine order
F	thrust
H	fan annulus height
L	inlet length
N	fan rotational speed
P _S	static pressure
P _T	total pressure
S0	short undrooped inlet
SOV	short undrooped inlet with variable-inlet guide vanes
V	velocity

¹ Detail results of the test are unpublished data at the NASA Lewis Research Center.

W_C airflow corrected to sea level standard conditions
 X longitudinal dimension from inlet leading edge
 Y vertical dimension from duct wall
 α inlet angle-of-attack (nacelle incidence)
 β variable-inlet guide vane setting angle
 θ total temperature ratio
 θ_{wall} diffuser wall angle

Subscripts

F fan
 H highlight
 L local
 M maximum
 Sep separation incidence
 T throat
 1 probe indicator (location shown in fig. 9(a))
 2 inlet rake station
 3 fan exit station
 4 probe indicator (location shown in fig. 9(a))
 ∞ free stream

APPARATUS

Test Facility and Model

The investigation was conducted in the NASA Lewis 9- by 15-ft (2.743- by 4.572-m) Low-Speed Wind Tunnel, an essentially atmospheric tunnel with a free-stream velocity range of 0 to 145 kn (74.6 m/sec). A complete description of the tunnel and its aerodynamic characteristics is contained in reference 4.

The model installed in the test section of the 9- by 15-ft (2.743- by 4.572-m) tunnel (ref. 5) is shown in figure 1. It is supported by a horizontal strut (hidden from view) and a vertical pipe stand and is rotated in a horizontal plane for angle-of-attack variation. The strut houses the ducting of the turbine-drive air to the fan, instrumentation lead lines, and hydraulic lines.

The three mated model components, namely the inlet, the VIGV subassembly, and the 20-in.- (0.508-m-) diameter fan are shown in figure 2.²

Inlet system. - The inlet (including the six-spoke rake assembly) is the same as the short inlet installation (SO), which was previously investigated during an earlier inlet test program. Salient features of the inlet are given in figure 3. The steady-state pressure instrumentation consisted of axial rows of static pressure taps at four circumferential locations. These locations were instrumented as follows: the windward side, 0° with 25 static pressure taps; the leeward side, 180° with 14 statics; and the 45° and 225° sides with 5 static taps each. Two additional static pressure taps at 90° and 270° were also installed 8 in. (20.32 cm) downstream of the highlight.

Six equally spaced rakes consisting of 19 total pressure taps and 2 free stream static pressure taps were mounted at the inlet diffuser exit station just forward of the VIGV assembly, figure 4(a),(b). Seven wall static pressure taps were contained in the outer wall ring which formed part of the duct at the rake station. This instrumentation provided total pressure recovery, distortion, flowrate, and indications of flow separation at the diffuser exit just ahead of the entrance to the VIGV assembly. The first and fourth total pressure taps (counting from the outer wall of the bottom windward rake) were individually connected to two separate differential pressure transducers. The nearest wall static pressure was connected to the other side of the transducers to serve as flow separation indicators, figure 4(c). When the pressure difference was negative, the flow was called separated. Their outputs were recorded on an x-y plotter and also displayed on panel meters in the control room during the test.

The inlet configuration code contains the following three parameters: the first is the length of the diffuser, S is for short; the second is the droop of the inlet, O is for a no-droop inlet; and the third indicates whether or not the VIGV assembly is present, V indicates a configuration with the VIGV assembly. Consequently inlet SOV refers to the inlet with a short diffuser, 0° droop and VIGV assembly. Throughout this report, the SOV inlet will be compared with the previously tested SO inlet.

Variable-inlet guide vanes (VIGV). - The VIGV subassembly has 20 full-span vanes of NACA-63-009 series profile. The front portions of the vanes are fixed and only the rear portions are rotated to change vane angle. A photograph of the subassembly and its actuation mechanism is shown in figure 5. The centerbody extends slightly upstream of the inlet throat. Because the VIGV's were taken from another model, their span was longer than if they had been specifically designed for the present test. Consequently the diameter of the centerbody at the leading edge of the VIGV's (the diffuser exit plane for the SOV inlet) was smaller than the diameter at the diffuser exit plane for the SO inlet. This difference resulted in a flow area at the diffuser exit of the present configuration (SOV) that was larger than the diffuser exit flow area of the model tested earlier (SO). The resulting area distribution for both inlets is shown in figure 5(b).

²Hamilton Standard VIGV's for GAC Inlets at the NASA Lewis Research Center, Modification Drawings Nos. 698 MOD 2580C-2592. Aero Test, Grumman Aerospace Corporation, January 1979.

Fan. - The single stage 20-in.- (0.508-m-) diameter fan has 15 circular arc rotor blades and 25 stator blades with a rotor-stator spacing of one rotor-tip chord length. During this test the rotor blades were set at the design setting angle of 27° relative to the axial direction. The fan is powered by a four-stage turbine. The turbine is driven by heated, high pressure air fed through passages in the model support strut and pylon. At its nominal design speed of 8020 rpm the fan pressure ratio is 1.17 and may be operated to a speed of 120 percent with a pressure ratio of 1.25. Reference 5 gives a more complete description of the fan and its aerodynamic performance.

The flow characteristics through the fan are determined from pressure and temperature instrumentation at the fan stator exit, figure 4(d). Turbine exit pressures and temperatures are also recorded. Vibratory stresses were monitored with strain gages located at discrete locations on the fan rotor, stator, and turbine; thereby insuring the safety of the fan during the test.

Test Procedures

Before each new operating condition of constant tunnel velocity, nacelle angle, VIGV setting, and fan speed, a safety sweep was made. This sweep consisted of monitoring the blade stress as either the VIGV setting or the fan speed was continuously varied from the lowest to highest value. If the stress levels approached the upper allowable range of operation, then testing was terminated to preclude damage to the fan. Monitoring of the inlet flow separation parameters and rotor blade strain gages helped evaluate the cause for the blade stresses; that is, whether the cause was induced by inlet flow separation or fan stall. Data were then recorded at discrete (safe) VIGV and/or fan speed settings. Fan blade stresses were observed on a spectrum analyzer in the control room and the unfiltered root mean square signal from the strain gages was also displayed on a x-y plotter as a function of VIGV setting or fan speed. Internal flow separation indicators were similarly displayed for the first and fourth probes as described previously.

Test Schedule

A run schedule is shown in table I. Only one of three originally proposed test groups were completed (i.e., fan nozzle exit area 100 percent of design). Two smaller fan exit nozzles (96 and 92 percent of the design exit area) were tested for NASA-related control studies which are not reported here. However, the aspects of these test groups which apply to VIGV-fan-stage performance are covered in the discussion of the test results.

TEST RESULTS

The test results show the effects of the variable-inlet guide vane installation on the performance and angle-of-attack capability of the inlet system, the fan-stage performance, and the aeromechanics of the fan blades. Results are shown at combinations of free stream velocity and nacelle angle-of-attack that would be encountered during the aircraft transition from takeoff to cruise or cruise to landing. The discussion includes the following:

(1) Performance of the short inlet with VIGV's (SOV) compared to the performance of the short inlet without VIGV's (SO). This comparison shows the effects of the VIGV installation on inlet performance and angle-of-attack capability.

(2) Thrust modulation of the inlet VIGV system at constant fan speed for each test condition of free stream velocity and nacelle angle-of-attack.

(3) Effect of fan nozzle exit area variation on the thrust modulation capability of the inlet VIGV system.

Performance Comparison of SOV and SO Inlets

Pressure recovery and distortion. - Figures 6 to 8 compare the area-weighted average total pressure recovery (P_{T2}/P_T) and the distortion ($(P_{Tmax} - P_{Tmin})/P_{T2}$) as functions of specific airflow for the SO and SOV inlets with the VIGV angle set at zero degrees ($\beta = 0$). In horizontal flight ($\alpha = 0$), for free stream velocities ranging from 40 to 125 kn (20.6 to 64.3 m/sec), the VIGV installation imposes only a slight penalty in total pressure recovery and distortion, as indicated in figure 6. However, under transition conditions, shown in figures 7 and 8, the SOV inlet shows lower pressure recoveries and higher distortions than the SO inlet configuration. These performance losses are amplified whenever poor flow conditions exist. Poor flow conditions are due to the combined effects of any localized blockage of the flow which is caused by the presence of the VIGV's and/or the more severe VIGV area distribution (fig. 5(b)) in the already sensitive 12° -wall-angle diffuser. Since the total pressure rake that measures inlet performance is located upstream of the VIGV vanes, any measured pressure loss is not due to the direct viscous losses of any phenomena occurring on the vanes, but rather caused by losses that occur in the diffuser wall boundary layer. These boundary layer losses may be due to adverse turbulent disturbances propagated upstream from the VIGV installation or caused by an increased adverse pressure gradient owing to the difference in flow area throughout the diffuser (as shown in fig. 5(b)). Although the increased pressure gradients associated with the SOV diffuser are not much larger than those in the SO diffuser, the inlet is operating at conditions of incipient separation when separation limits are determined, and consequently small changes in pressure gradient could have a major effect on inlet total pressure levels.

Angle-of-attack. - The inlet angle-of-attack capability at a given free stream velocity is defined as the locus of nacelle angles-of-attack for which the boundary layer of the inlet airflow just attaches to the inlet. It is obtained either by (1) increasing power setting (airflow) at constant nacelle angle-of-attack and VIGV angle, (2) by reducing nacelle angle-of-attack at constant VIGV angle and power setting, or (3) by reducing VIGV angle at constant nacelle angle-of-attack and power setting. In all three procedures the attachment point is approached from the separated flow regime. Flow was considered to have attached at the point where the separation parameter ($P_{T1} - P_S$) or ($P_{T4} - P_S$) became positive. Use of the total pressure probe closest to the wall ($P_{T1} - P_S$) results in a lower angle-of-attack capability. The parameter which best predicts the impact of the inlet on engine or fan performance depends on the distortion tolerance of the specific engine or fan being used. The angle-of-attack capability, up to free stream velocities of 125 kn

(64.3 m/sec) for the SO and SOV inlets (which utilize the first probe parameter), is shown in figures 9 and 10(a) respectively. The first probe parameter results of the SOV inlet are presented for a range of β 's in figure 10(a) to (e) while the fourth probe parameter results are presented in figures 11 and 12(a) to (e). There was no obvious trend of airflow with variations of vane settings for particular inlet angles-of-attack separation angles. As a consequence, individual data points were not plotted. The variation of the airflow with β is indicated by bars in the figures 10 to 12. Either these β trends were very complicated or else a weak trend could have been masked by a random variation of the conditions where separation first occurs. To evaluate the reasons for the spread in the data, enough data would have to have been taken to determine a statistical average. Scheduled tunnel occupancy time did not permit this approach. However to compare SOV inlet data directly with SO data a curve was faired through the $\beta = 0$ data points. Figures 9, 10(a), 11, and 12(a) show the SO and SOV capability separately for clarity while figures 10(b) to (e) and 12(b) to (e) show SO and SOV inlet comparisons at specific velocities. Both sets of data show a substantial angle-of-attack capability loss for the VIGV configuration (SOV).

The first probe parameter shows a loss in angle-of-attack capability for the SOV inlet ranging from 26° to 35° at 40 kn (20.6 m/sec) (fig. 10(b)) and 12° to 18° at 125 kn (64.3 m/sec) (fig. 10(e)). These values amount to roughly 40 percent of the SOV inlet angle-of-attack capability and 30 percent of the SO inlet angle-of-attack capability. The corresponding range in angle-of-attack loss using the fourth probe parameter (figs. 11 and 12) are 13° and 29° at 40 kn (fig. 12(b)) and 7° to 15° at 125 kn (fig. 12(e)). Again the separation of the boundary layer in the diffuser at lower inlet angles-of-attack is thought to be caused by the presence of the VIGV's and/or the more severe inlet area distribution.

An interesting observation on figures 10 and 12 is that VIGV actuation (i.e., $\beta > 0^\circ$) results in only a minor effect on the angle-of-attack capability. Also, the minor changes that do occur in the angle-of-attack limit do not seem to vary in a consistent manner with a β variation. As an example, it can be seen from figure 10(b) that at a low mass flow with $\beta = 30^\circ$ the angle-of-attack limit is improved roughly 5° with respect to the $\beta = 0^\circ$ value, but at intermediate mass flows the $\beta = 30^\circ$ angle-of-attack limit is roughly 10° lower than the $\beta = 0^\circ$ value. Since (1) the larger deflection angles of the VIGV vane would result in additional flow blockage within the vane passages and (2) it was observed in figures 10(b) to (e) that increasing the VIGV deflection angle results in only a minor effect on the angle-of-attack capability, it is somewhat doubtful that VIGV blockage alone is responsible for the loss of the limiting angle-of-attack of the SOV inlet.

Diffuser exit boundary layer. - The evaluation of V/STOL inlets depends on whether or not there exists separated flow at the fan face. Two different evaluators have been presented herein to determine whether or not separation exists. One is the difference between the pressure on the first total pressure tube on the windward rake and the closest static pressure. The second is the same except the fourth total pressure tube is used. Consequently, since the angle-of-attack capability of an inlet is sensitive to whether a fourth tube or first tube indicator is used in the evaluation, an examination of the boundary layer profile is needed in light of the two separation indicators.

The boundary layer characteristics at the windward rake station of the SOV inlet are compared with the SO inlet in figure 13. The same transition flight conditions are used here that were used to compare the pressure recoveries and distortions of these two inlets in figures 7 and 8. The boundary layer profiles for the SO and SOV inlets are shown for roughly the same airflow at 40 kn (20.6 m/sec) and $\alpha = 90^\circ$ in figure 13(a). The SO inlet boundary layer profile at the diffuser exit (fan face) indicates attached flow, while the SOV inlet profile shows separation with reverse flow. The first probe separation indicator of the SOV inlet shows the flow as being fully separated. The fourth probe indicator shows the flow just attached. (The fourth probe's total pressure is equal to wall static pressure.) In another example at 60 kn (30.9 m/sec) and $\alpha = 90^\circ$, figure 13(b) shows that the flow is separated by using either the first or the fourth probe indicators even though the profiles of both cases look quite similar. Boundary layer profiles for 80 kn (41.2 m/sec) at $\alpha = 60^\circ$ and for 125 kn (64.3 m/sec) at $\alpha = 45^\circ$ are shown in figures 13(c) and (d) respectively. On figure 13(c) both the first and fourth tube evaluators indicate separation with the SOV inlet, while neither indicate separation with the SO inlet. On figure 13(d) only the first tube evaluator indicates separation, even though the velocity of the reverse air flow within the separation region appears to be greater than the velocity within the separated region of figure 13(c). The selection of the indicator used may depend on the particular inlet-engine configuration that is being contemplated. It is interesting to note that even with the highly distorted flow profile in figure 13(c), where pressure losses extend to approximately 50 percent of the diffuser exit passage height, the blade stresses were within acceptable limits. (Blade stresses are shown in figs. 15 and 16.)

To further investigate the difference of the flow between SO and SOV inlets, a comparison was made of the static pressures in the diffuser along the windward meridian. Figure 14 presents static pressure profiles for those operating points appearing in figure 13; that is, data that has essentially the same corrected weight flow for a particular transition flight condition. There seems to be two basic locations in the diffuser where there exist unexpected inflections in the static pressure profiles. One location is between X/D_F of 0.15 and 0.2; that is, near the minimum geometric area of the duct without the centerbody. The other occurs between 0.275 and 0.4; that is, near the minimum flow area. (See fig. 5(b).) The disturbance near the minimum of the duct area is probably a local perturbation that originates because of local increases in the flow velocity caused by over expansion. The disturbance originating near the minimum flow area is undoubtedly due to boundary layer separations. The static pressure at this condition in turn would be sensitive to changes in the effective flow area. By comparing data of the SOV inlet with data of the SO inlet (fig. 14(a)) for a transition condition of 40 kn (20.6 m/sec) at $\alpha = 90^\circ$ with W_C/A_H approximately 0.1, it can be seen that the SOV inlet has a slightly different static pressure profile than the SO inlet. The rake profiles (fig. 13(a)), taken at roughly station 0.75, show a separation (fourth probe) existing with the SOV configuration and none for the SO configuration at these conditions. A disturbance is noticeable from the static pressure profile of the SOV inlet between stations 0.35 and 0.54. No disturbance is noticeable for the SO inlet. This supports the deduction that the downstream disturbance exhibited on the static pressure profiles is due to boundary layer separation. A similar observation can be made at a transition condition of 60 kn (30.9 m/sec) and $\alpha = 90^\circ$ (fig. 14(b)). The boundary layer profile presented in figure 13 indicates that the separation for the SOV inlet is larger

at these transition conditions than the SOV inlet separation for the case presented in figure 14(a). The fourth probe indicates unconditional flow separation with even flow reversal. In this case, the boundary layer separation extends upstream ahead of the minimum flow area. In figure 14(d) where the fourth probe indicator indicates attached flow, the static pressure profiles indicate that separation extends just up to the minimum flow area.

Data for the SO inlet at various weight flows is also presented on figure 14(d) to show the effect of decreased weight flow. The flow is definitely attached at W_L/A_H values of 0.163 and 0.145. At a value of 0.121 the flow is separated by the first probe indicator but attached by the fourth probe indicator, as can be seen from figure 13(d). Although it is difficult to tell the exact nature of the flow from the static pressure profile, one can see the disturbances. One can conclude from the above observations of the diffuser static pressure ratio that a thickening boundary layer occurs when the fourth probe data indicates separation. This thickening is substantiated from the static pressure profile. The profiles indicate that the disturbance starts at the minimum flow area. The larger the extent of the diffuser exit separation, determined from fourth probe data, the farther upstream the boundary layer disturbance originates.

Fan blade stresses. - Fan rotor blade stresses are recorded in real time on an x-y plotter during the test as a safety parameter for fan operation. The stress plots reflect the total unfiltered root mean square signal from the strain gage; the major component is the first flatwise bending mode. Stress spikes on the plots occur at specific engine order revolutions per minute where the blades vibrate at their resonant frequency. These engine orders (EO) are defined as an integral number of blade vibratory cycles per fan revolution.

In horizontal flight ($\alpha = 0^\circ$), the SOV inlet showed higher stress levels than the SO inlet and also showed a change in the character of the stress signature, figure 15(a) to (c). Inlet SOV has higher EO3 stresses and in addition has a stress spike at EO4 not generally present with the SO inlet at the same conditions, except at extreme transitional flight conditions, as shown in figures 16(c) and (e).

At transition flight conditions the SOV inlet stresses are generally much higher than for level flight, even for $\beta = 0$, and are sometimes more than a factor of two as shown on figures 16(a) to (i). Actuation of the VIGV further increases blade stresses at forward speeds up to 80 kn (41.2 m/sec), but the increase is not evident at higher speeds. There is no overall simple variation in blade stress with changing VIGV setting. The relationship must be categorized according to tunnel air velocity. At 80 kn (41.2 m/sec) or less, VIGV blade angle has no effect on the EO4 blade stress. At EO3 and $\beta = 40^\circ$ the blade stress is roughly double the value that occurs for $\beta = 0^\circ$. (See figs. 15(a) to (c) and 16(a), (b), and (d).) At 125 kn (64.3 m/sec) the overall blade stress decreases as β increases. (See figs. 15(d) and 16 (h).)

Effect of VIGV on Fan Performance

Fan performance with VIGV actuation was obtained at constant fan speeds of 110 and 70 percent of design and, wherever possible, other speeds depending on tunnel speed and nacelle angle-of-attack conditions. Airflow and thrust

modulation capability within the inlet-VIGV-fan compatibility range are discussed.

Airflow modulation. - The VIGV airflow modulation characteristics are presented in figures 17(a) to (n) for all the combinations of V_∞ , α , and fan speed conditions tested. The maximum airflow obtainable by reducing β is limited as evidenced by the negligible increase in airflow from $\beta = 0^\circ$ to $\beta = -5^\circ$ (figs. 17(a) to (d), (f), (g), and (j)).

There are several explanations as to why the flow is limited. One is that the flow in the VIGV passage could be choked. Another is that the effects of the swirl produced by the VIGV's could be so great that the relative angle-of-attack of the rotor blade exceeds its limits and partially stalls the fan. The flow over the rotor blade would consequently separate and cause an effective area restriction. Additional data above that available in this report would be necessary to determine the source which limits the flow.

The minimum weight flow obtained by increasing β may be limited by fan stall or by inlet separation. Fan stall was determined by a sudden change in revolutions per minute caused by a change in the loading of the fan or a change in fan noise level. Observable fan stall only occurred at static conditions as indicated in figure 17(a).

At zero angle-of-attack, the inlet did not separate at any air flow condition. As the angle-of-attack increased, the inlet separated. The separation bounds from the first and fourth probe indicators are superimposed on figures 17(c) to (e), (g) to (k), (m), and (n). The first probe indication is the more conservative and limits usable operation to the higher airflows. Since the separation lines are nearly vertical, the minimum airflow for any combination of V_∞ and α is almost independent of the VIGV setting.

Thrust modulation. - The range of available fan thrust (as calculated from the inlet weight flow, fan discharge pressure, and temperature) for the VIGV inlet assembly at 110 percent fan speed is presented in figure 18 as a function of VIGV vane setting, nacelle angle-of-attack, and flight velocity; the zero velocity (static or hover condition) data are also presented as a scale on figure 18(a). The thrust for static conditions varies from 26500 N/m² (553 lb/ft²) to 5985 N/m² (128 lb/ft²) of fan disk area which was obtained by varying the VIGV setting from -5° to $+37.1^\circ$. This thrust range represents a modulation of 112 to 28 percent of design thrust. (Design thrust is that obtained at $V_\infty = 0$ and 100 percent fan speed.) At 70 percent design fan speed (fig. 19) the VIGV range is from -15° to $+40^\circ$ which corresponds to 58 to 22 percent of the value of the design thrust.

Figures 18 and 19 show that the full thrust range is limited by the inlet separation boundary. For example at $V_\infty = 40$ kn (20.6 m/sec) and the 110 percent fan speed (fig. 18(a)) both fourth and first probe boundaries are shown. The first probe boundaries are much more restrictive than the fourth probe criteria. The first probe limits full VIGV modulation ($\beta = 40^\circ$) to about $\alpha = 66^\circ$, limits β to 34° at $\alpha = 90^\circ$ (47 percent design thrust), and limits β to 22° at $\alpha = 120^\circ$ (80 percent design thrust). The fourth probe is considerably less restrictive allowing the full VIGV modulation up to 105° and only limiting β to 35° at $\alpha = 120^\circ$ (38 percent of design thrust). Again the separation criteria to be used will depend on the tolerance of the specific fan or engine under consideration. Because of very limited data with the fourth

probe separation indicator, only the first probe separation indicator is presented in the remainder of figure 18. Figures 18(c) to (e), show the available thrust range for 110 percent fan speed at the free stream velocities tested which incorporated the first probe separation criteria. The available thrust for 70 and 56 percent fan speed can be determined from figures 19 and 20 respectively.

Effect of Fan Exit Area

Two smaller fan exit nozzles, with area 96 percent (221 in.²) and 92 percent (212 in.²) of the design nozzle exit area of 230 in.² (0.148 m²), were used to investigate fan stall characteristics with VIGV actuation. Figures 21(a) to (e) present the thrust modulation with VIGV setting angle at two constant fan speeds, 110 and 70 percent of design, for a V_∞ at α test conditions of 0 kn at 0°, 40 kn at 0°, 125 kn at 0°, 40 kn at 90°, and 125 kn at 30° (0 m/sec at 0°; 20.6 m/sec at 0°, 64.3 m/sec at 0°, 20.6 m/sec at 90°, and 64.3 m/sec at 30°, respectively). Solid symbols denote the VIGV angles when fan stall occurred. As the fan exit area is decreased, the VIGV angle where the fan stall occurs decreases and the range of thrust modulation also decreases. At the $V_\infty = 0$, $\alpha = 0^\circ$ (fig. 21(a)) condition the decrease in thrust modulation range between the 230 and 212 in.² (0.148 and 0.137 m² respectively) exit area configuration is 29 percent. As the exit area is decreased the fan operating line will move closer to the stall line which in turn reduces the range of VIGV actuation. At 110 percent design speed the data presented in fan map format (fig. 22) shows the effect of VIGV actuation on fan stage performance. For comparison, the $\beta = 0^\circ$ data is plotted with the estimated stall line in figure 23. Data were not taken at any weight flow less than where stall occurred, so that only limits of stall operation and stall free-fan operation were recorded. Since the only fan stall at the design exit area was observed to have occurred during static conditions (see figs. 17(a) and 18 (a)), the nacelle angle-of-attack with the concomitant larger distortion did not create flow conditions that stalled the fan. The fan operated stall-free even when the inlet flow was separated at 40 kn at 90° and 40 kn at 120° (20.6 m/sec at 90° and 20.6 m/sec at 120°, respectively). The only factor that prevented data from being taken during nonhover flight conditions was high fan-blade stress levels.

The limitation of the positive VIGV range with decrease in fan exit area caused by fan stall or, as shown earlier, to inlet separation at high nacelle angles-of-attack, suggests that in order to alleviate this limitation, and consequently increase the range of thrust modulation, the fan exit area could be simultaneously increased as the VIGV is actuated closed. This concept was considered in reference 1; data from that reference is reproduced in figures 24(a) and (b) to illustrate the point. The two different types of aforementioned operating lines are presented on the figure. It can be seen in figure 24(a) that the line representing a mode of fan operation with a constant exit area intersects the stall line near a β of 32.5° (approx. 35°). This limits the obtainable range of thrust modulation. However, if the exit area is varied, as well as the VIGV setting, the operating line can be kept as far from the stall line as is desired (for adequate stall margin). The new operating line thus increases the thrust modulation range with the VIGV assembly. The stall margin can also be controlled by increasing the fan speed. (See fig. 24(b).) At 100 percent of design speed, figure 24(a), the fan will stall at 40 lb/sec (18.14 kg/sec) flow which was obtained with the optimum fixed exit area at a

$\beta = 32.5^\circ$. At 120 percent of design speed, optimum fixed exit area and even a $\beta = 42.5^\circ$ (40 lb/sec) the fan will not stall. These techniques should be considered as part of a complete inlet-VIGV-fan performance evaluation for each V/STOL aircraft configuration whenever VIGV's are used.

CONCLUSIONS

The effects of a variable-inlet guide vane (VIGV) assembly upon the performance of an inlet-VIGV-fan system were experimentally evaluated in the NASA Lewis 9 x 15 ft wind tunnel. These effects were found to be detrimental to angle-of-attack capability compared with a similar inlet-fan system that was tested previously without the VIGV. The different evaluators used to assess the VIGV penalties were as follows: (1) actual inlet-separation angle-of-attack, (2) range of available thrust modulation, and (3) fan blade stress.

The following is a list of the important conclusions:

- (1) Testing demonstrated that the VIGV's are effective thrust modulators.
- (2) For static conditions at 110 percent fan speed, thrust variation from 122 to 27 percent was obtained at VIGV deflection angles of $\beta = -5^\circ$ to 37.1° . Reducing fan speed to 70 percent extended both the positive and negative ranges of the VIGV deflection angle.
- (3) Forward flight increases the positive VIGV actuation range.
- (4) Nacelle angle-of-attack at a given forward speed has a negligible effect on actuation range as long as the inlet flow is attached.
- (5) Inlet flow separation limits the VIGV actuation range at high nacelle angles-of-attack and high free-stream velocities.
- (6) The installation of the VIGV assembly, which resulted in a different inlet diffuser area distribution, demonstrated a large loss of transition flight angle-of-attack capability as compared to the same inlet without VIGV's. At 40 kn (20.6 m/sec) a loss of 26° to 35° was incurred, with a 12° to 18° loss at 125 kn (64.3 m/sec). These losses were respectively 40 and 25 percent of the inlet α capability of an inlet without VIGV's. Increasing the VIGV angle beyond $\beta = 0$ has little effect on separation.
- (7) The VIGV installation also resulted in generally higher blade stresses and the introduction of stresses at E04 which were not present at similar conditions on an inlet without VIGV's.
- (8) Decreasing the fan nozzle exit area limits the positive VIGV actuation. Data indicates that VIGV thrust modulation range may be optimized by using a variable area nozzle.

REFERENCES

1. Moore, Royce D.; and Reid, Lonnie: Aerodynamic Performance of an Axial-Flow Fan Stage Operated at Nine Inlet Guide Vane Angles. NASA TP-1510, 1979.

2. Moore, Royce D.; and Osborn, Walter M.: Aerodynamic Performance of a 1.38-Pressure Ratio Variable-Pitch Fan Stage. NASA TP-1502, 1979.
3. Johns, Albert L.; Williams, Robert C.; and Pontonides, H.C.: Performance of a V/STOL Tilt Nacelle Inlet with Blowing Boundary Layer Control. AIAA Paper 79-1163, June 1979.
4. Yuska, J.A.; Diedrich, J.H.; and Clough, N.: Lewis 9 x 15 Foot V/STOL Wind Tunnel. NASA TM X-2305, 1971.
5. Abbott, John M.; Diedrich, James H.; and Williams, Robert C.: Low-Speed Aerodynamic Performance of 50.8 - Centimeter-Diameter Noise - Suppressing Inlets for the Quiet, Clean, Short-Haul Experimental Engine (QCSEE). NASA TP-1178, 1978.

TABLE I. - RUN SCHEDULE^a

[Fan speed, percent of design; minimum, 20, 40, 60, 90, 100, and 110; VIGV angle, β , deg.: -10°, 0°, 10°, 20°, 30°, and maximum; fan nozzle exit area, 100 percent of design.]

Run	Nacelle angle-of-attack, α , deg	Tunnel speed, VX	
		kn	m/sec
1	0	0	0
2	0 60 90 120	40	20.6
3	0 60 90 120	60	30.9
4	0 45 60	80 80 80	41.2 41.2 41.2
5	0 30 45	125 125 125	64.3 64.3 64.3

^aTwo groups of smaller fan exit nozzles, (92 and 96 percent of design exit area) are not listed here.



FIGURE 1. - MODEL INSTALLATION IN NASA LEWIS RESEARCH CENTER LOW-SPEED WIND TUNNEL.

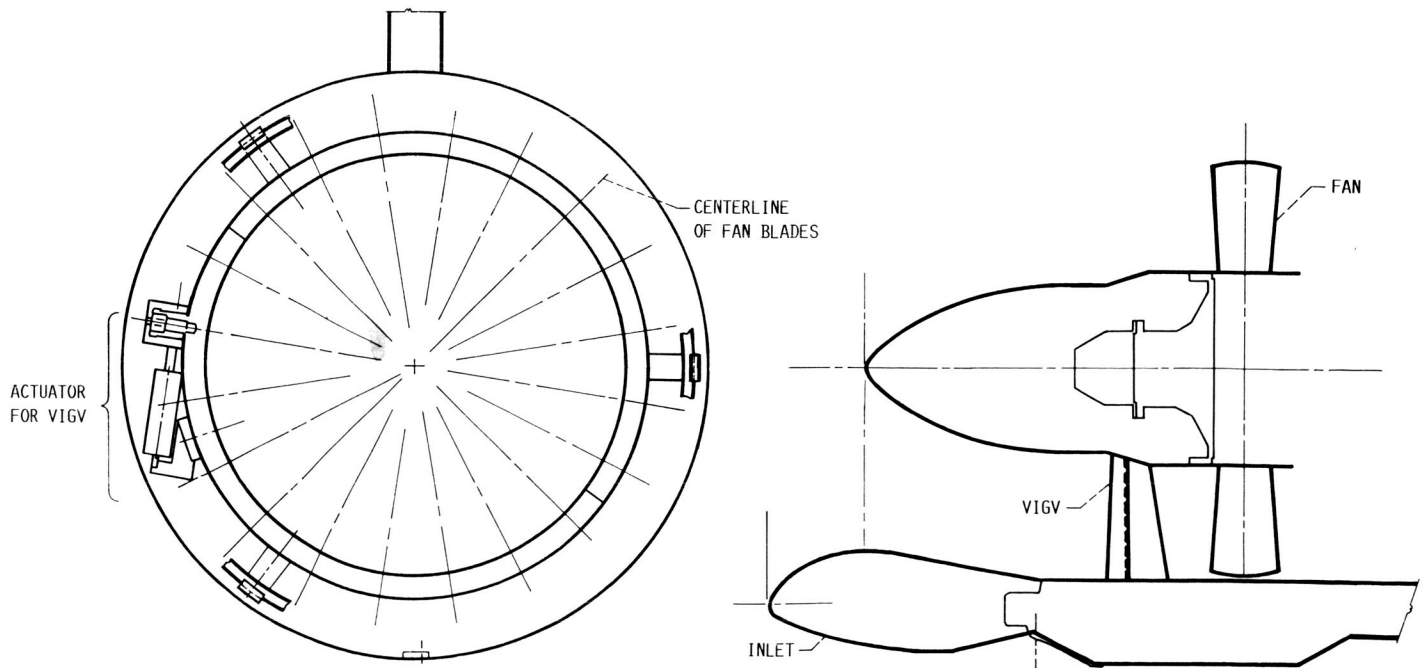
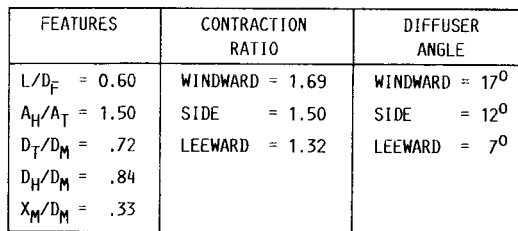
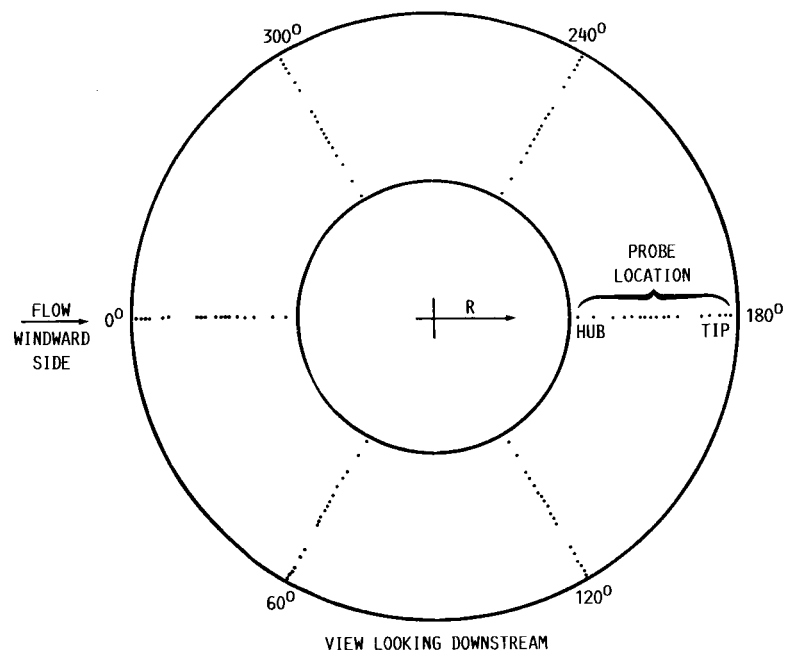


FIGURE 2. - SKETCH OF SHORT INLET WITH VARIABLE-INLET GUIDE VANES.



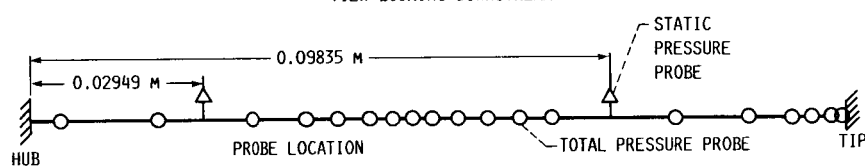
15



PROBE RADIUS AND WEIGHTED AREA OF EACH RING (TYPICAL FOR EACH RAKE)

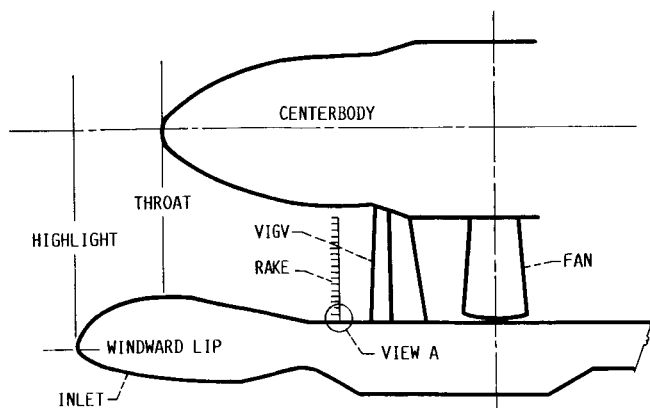
RING	RADIUS, R, M	$\Delta A/A_{TOTAL}^a$, PERCENT
HUB	0.1168	----
1	.1219	6.411
2	.1382	8.832
3	.1544	7.623
4	.1636	4.629
5	.1630	3.542
6	.1742	3.038
7	.1778	2.486
8	.1814	2.536
9	.1849	2.585
10	.1835	3.302
11	.1938	4.065
12	.1991	4.277
13	.2047	10.937
14	.2253	14.395
15	.2375	8.854
16	.2449	5.237
17	.2484	3.223
18	.2515	2.383
19	.2532	1.644
TIP	.2541	----

$A_T = 0.1600 \text{ m}^2$.

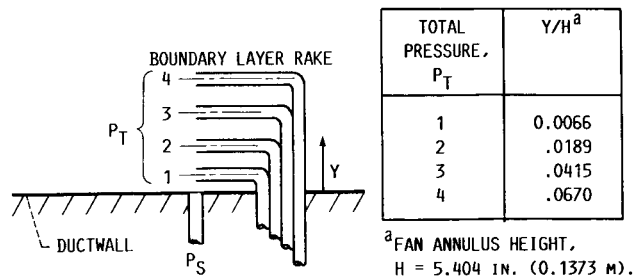


(A) FAN-FACE RAKE TOTAL AND STATIC PRESSURE INSTRUMENTATION.

FIGURE 4. - MODEL INSTRUMENTATION.



(B) CROSS SECTION VIEW.

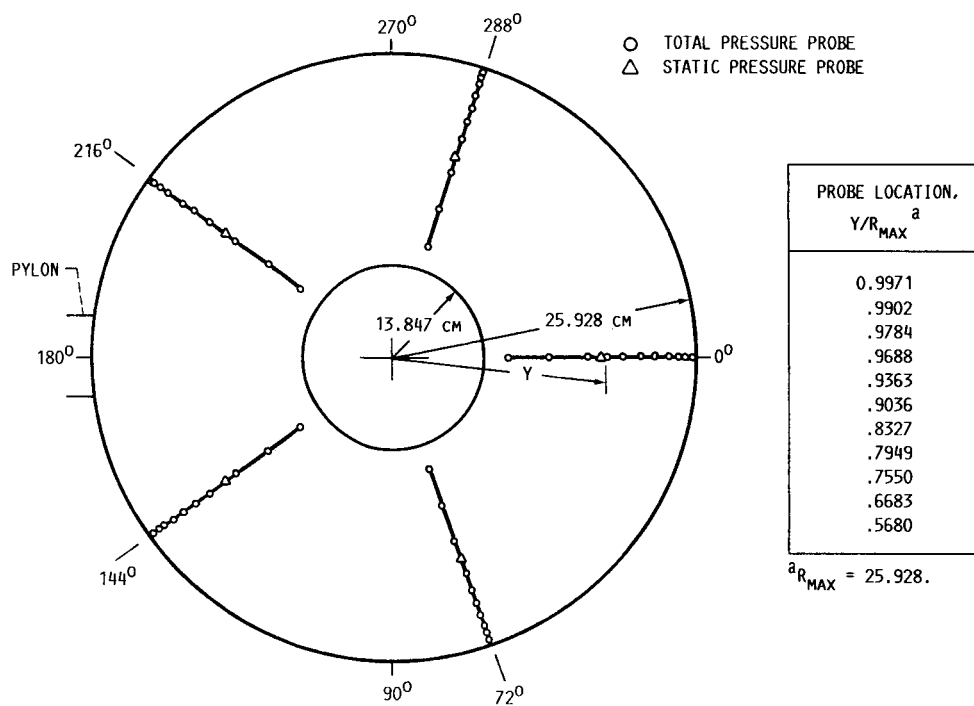


(C) VIEW A.

TOTAL PRESSURE, P_T	Y/H^a
1	0.0066
2	.0189
3	.0415
4	.0670

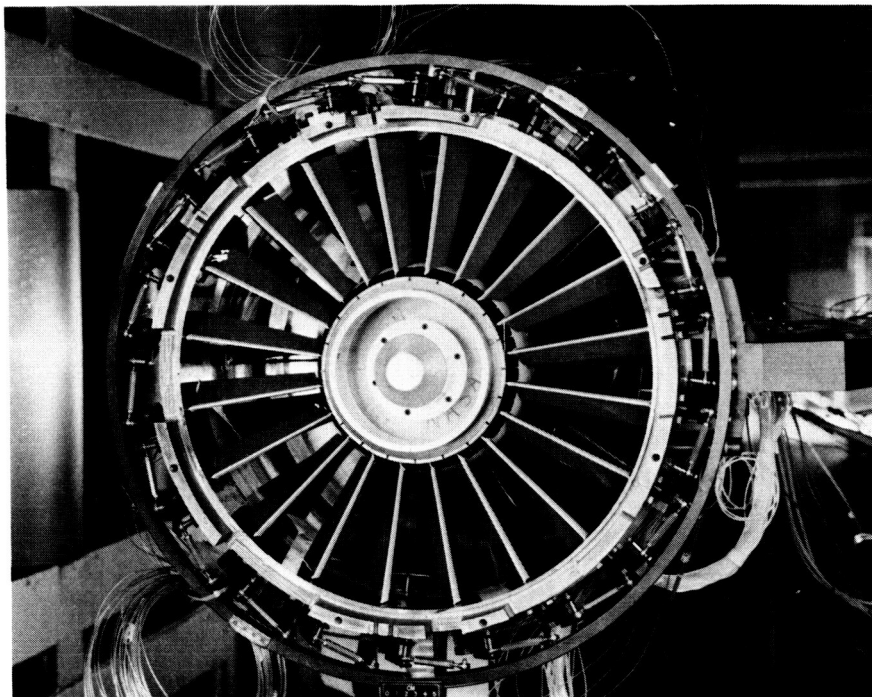
a FAN ANNULUS HEIGHT, $H = 5.404 \text{ IN. (0.1373 M)}$.

FIGURE 4. - CONTINUED.

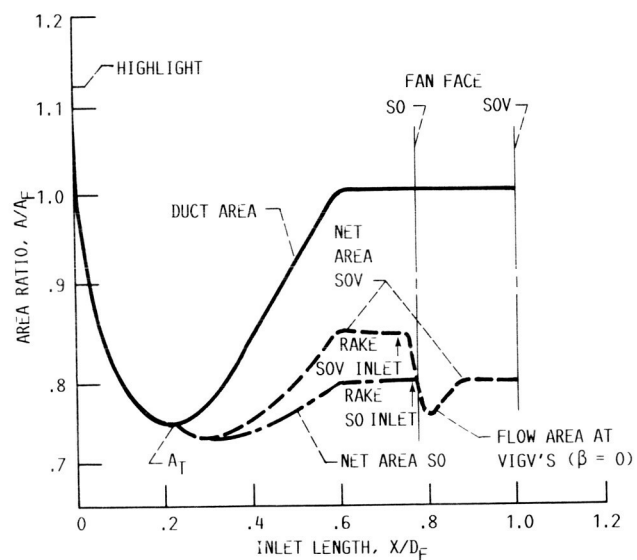


(D) FAN STATOR EXIT TOTAL PRESSURE INSTRUMENTATION, VIEW LOOKING UPSTREAM.

FIGURE 4. - CONCLUDED.



(A) VARIABLE-INLET GUIDE VANE SUBASSEMBLY INSTALLED.



(B) AREA DISTRIBUTION OF VARIABLE-INLET GUIDE VANE
INSTALLATION.

FIGURE 5. - VARIABLE-INLET GUIDE VANE INSTALLATION.

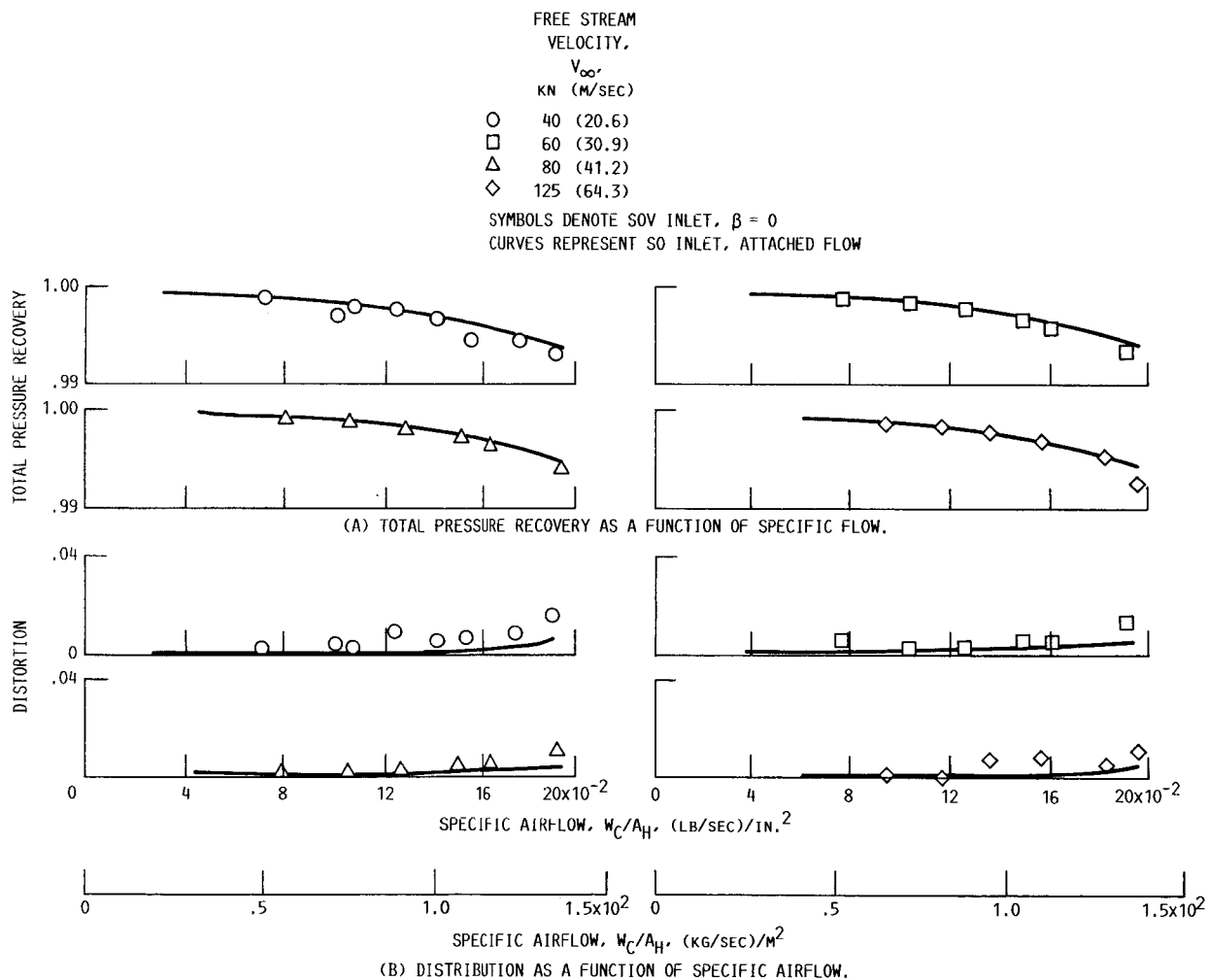


FIGURE 6. - VIGV INSTALLATION EFFECTS ON INLET PERFORMANCE AT $\alpha = 0$.

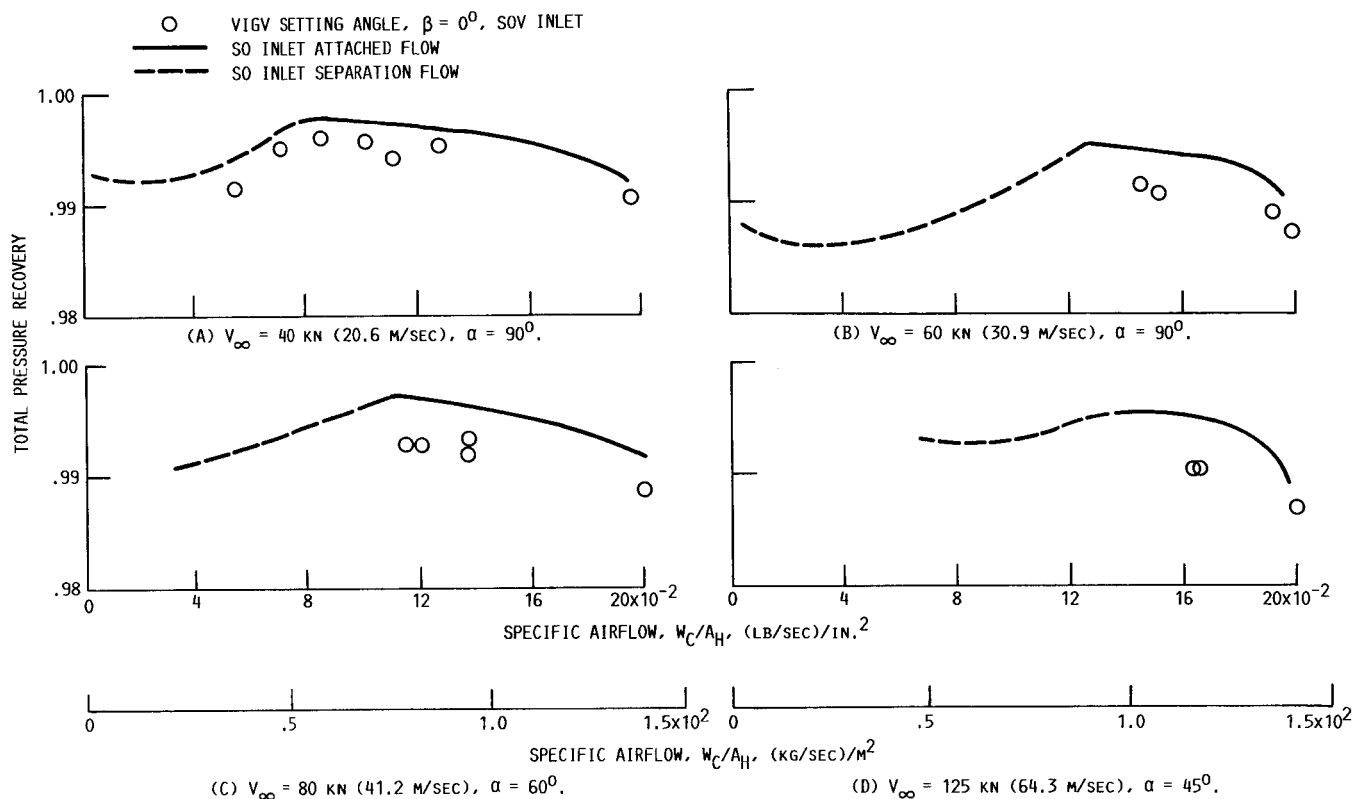


FIGURE 7. - TOTAL PRESSURE RECOVERY AS A FUNCTION OF SPECIFIC AIRFLOW AT TRANSITION FLIGHT CONDITIONS.

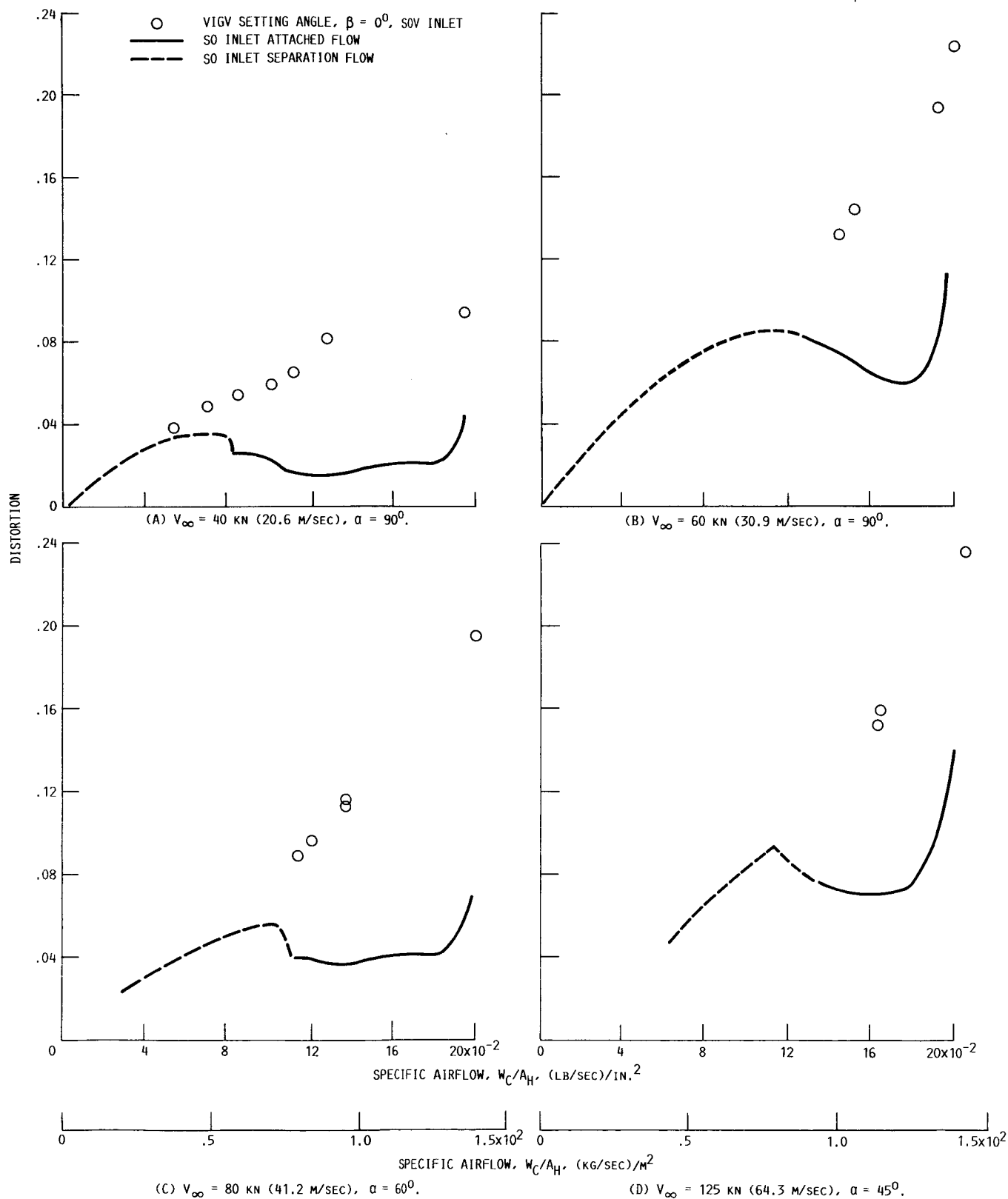


FIGURE 8. - DISTORTION AS A FUNCTION OF SPECIFIC AIRFLOW AT TRANSITION FLIGHT CONDITIONS.

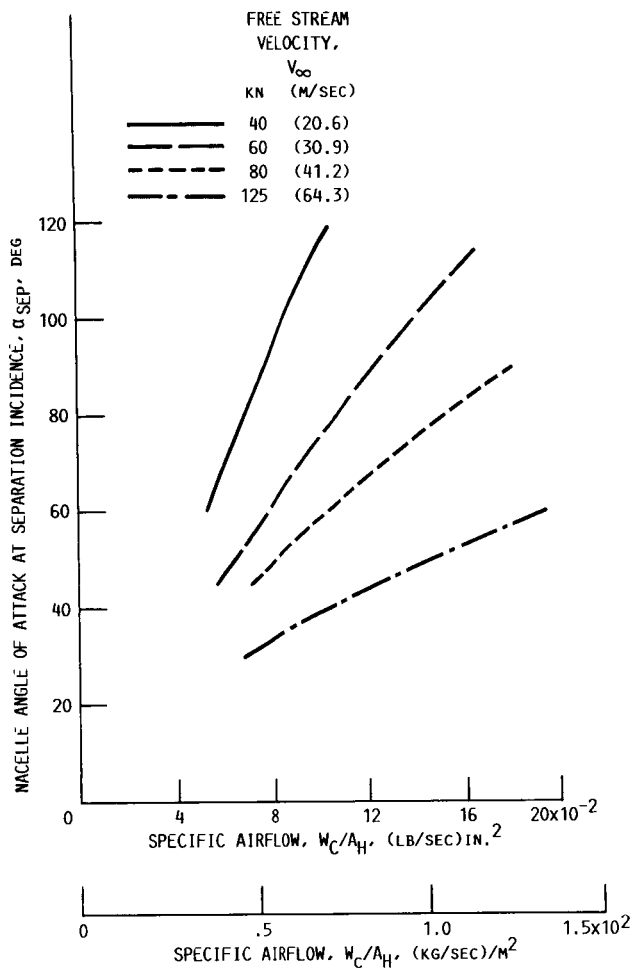
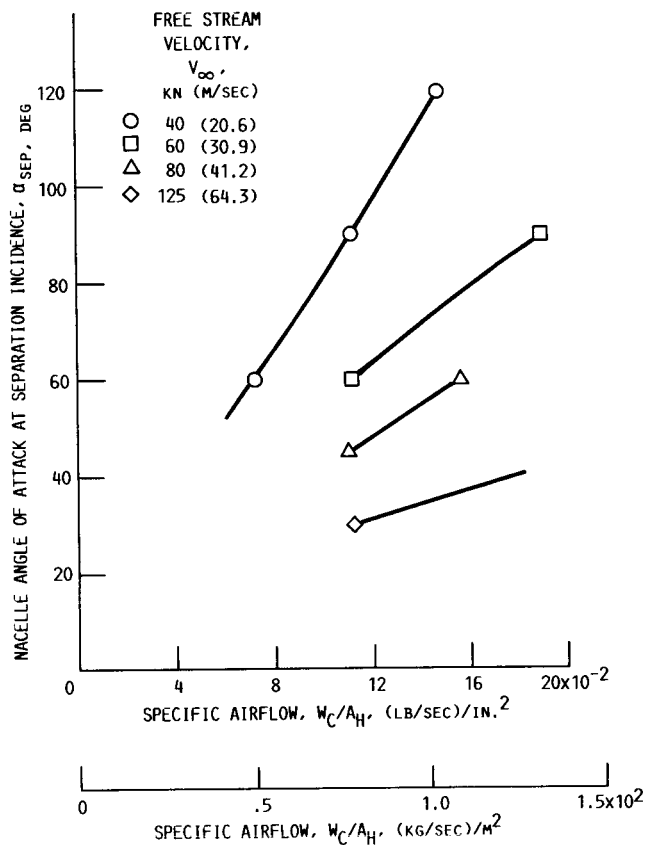


FIGURE 9. - SEPARATION BOUNDS OF SO INLET BASED ON $P_{T1} - P_S = 0$.



(A) INLET WITH VIGV SOV, VANE ANGLE $\beta = 0^\circ$.

FIGURE 10. - VIGV INSTALLATION EFFECTS ON SEPARATION BOUNDS BASED ON $P_{T1} - P_S = 0$.

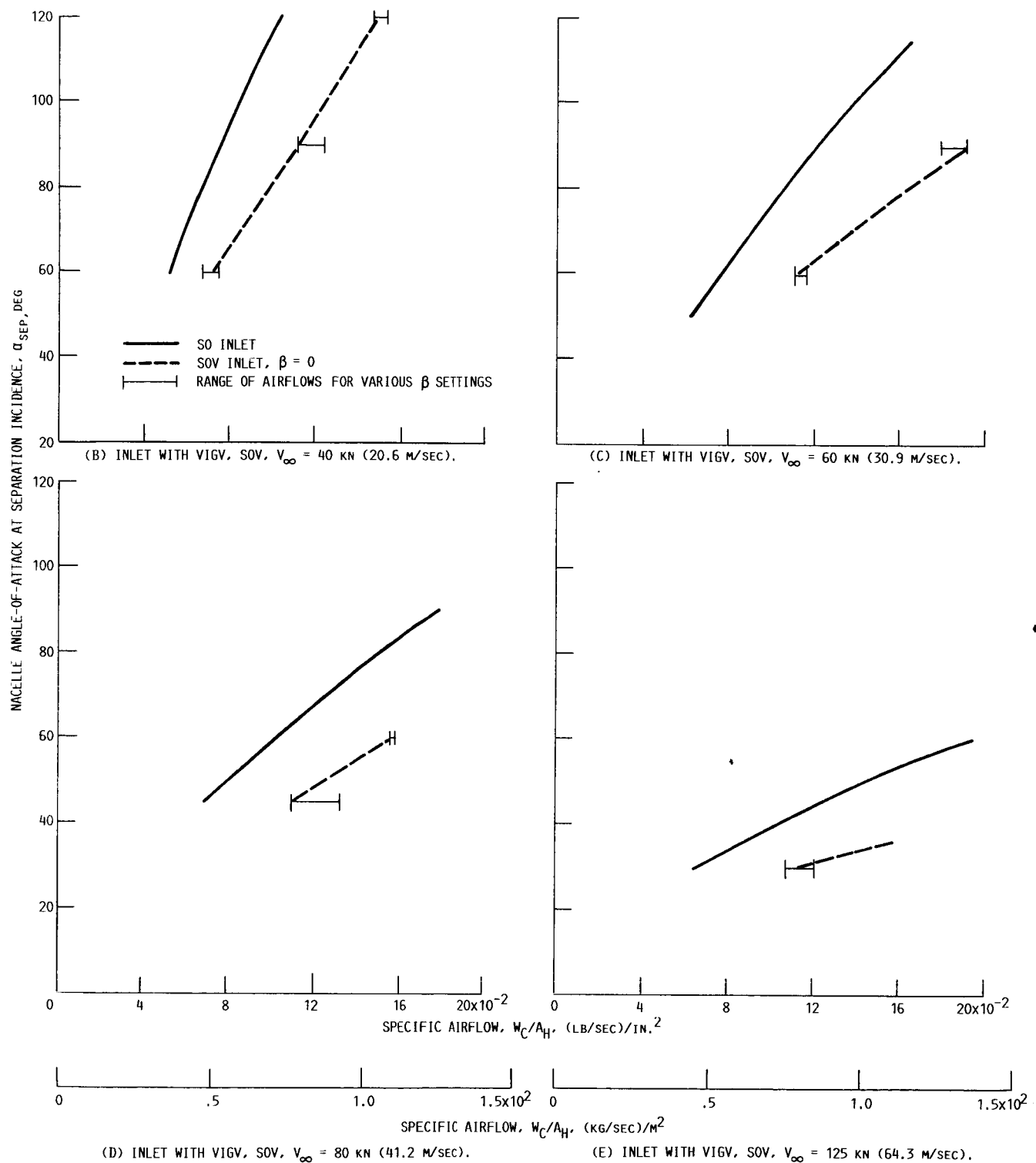


FIGURE 10. - CONCLUDED.

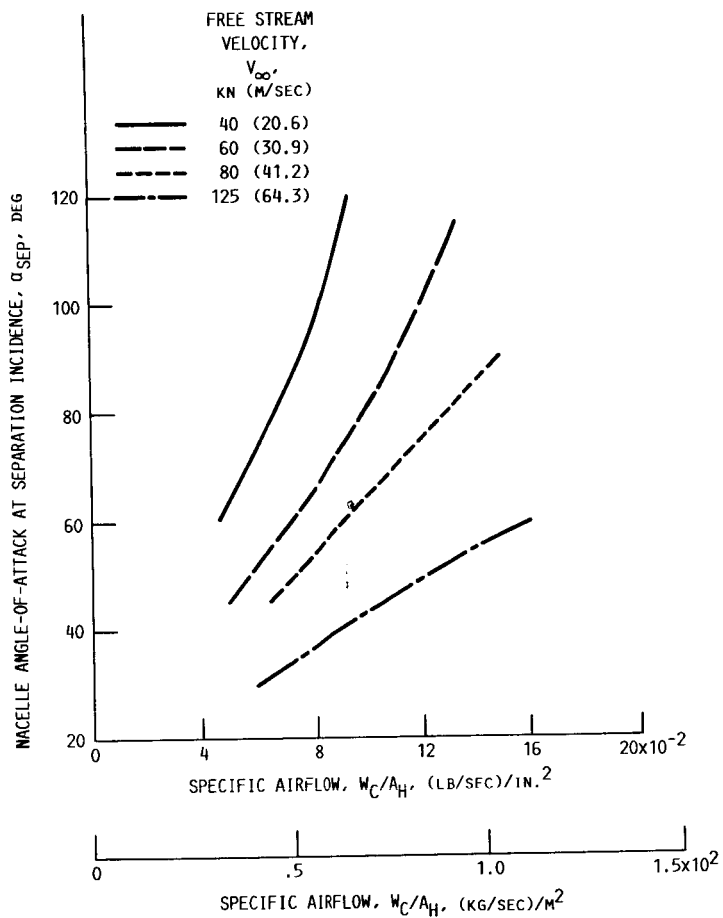
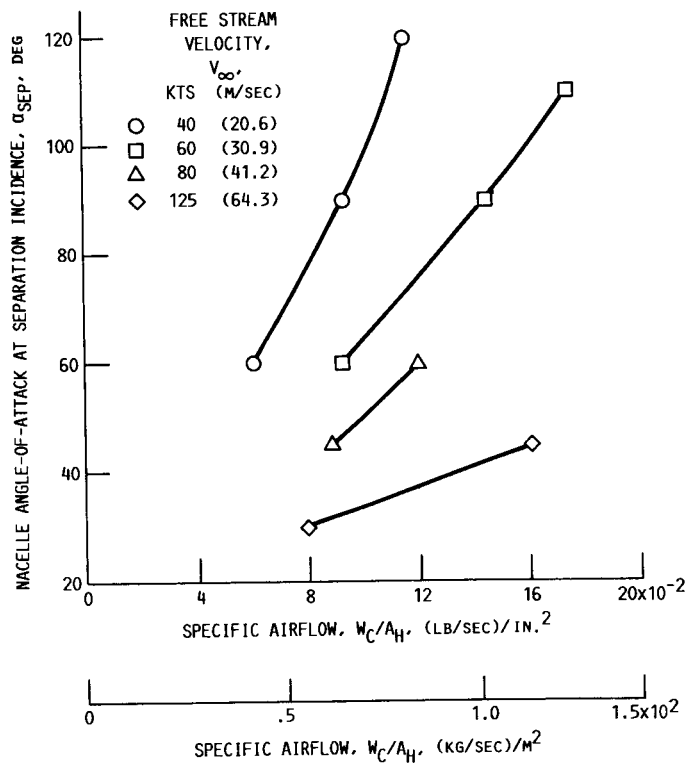


FIGURE 11. - SEPARATION BOUNDS OF SO INLET BASED ON $P_{T4} - P_S = 0$.



(A) INLET WITH VIGV, SOV; VANE ANGLE $\beta = 0^\circ$.
FIGURE 12. - VIGV INSTALLATION EFFECTS ON SEPARATION BOUNDS BASED ON $P_{T4} - P_S = 0$.

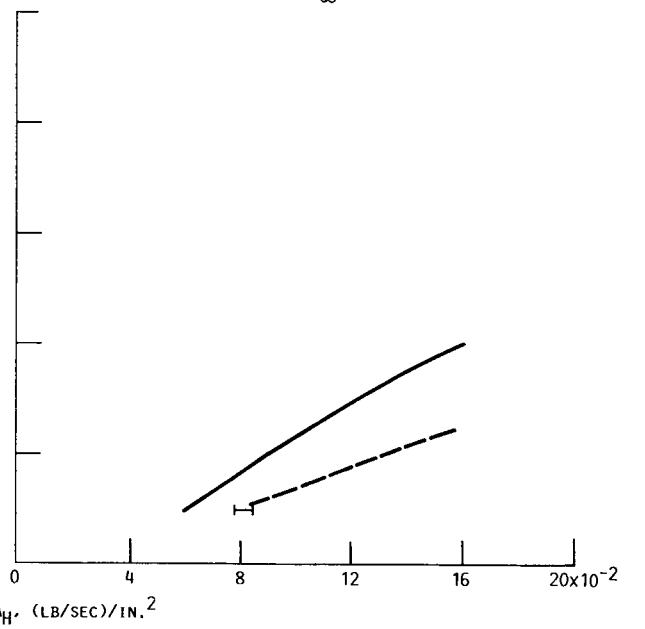
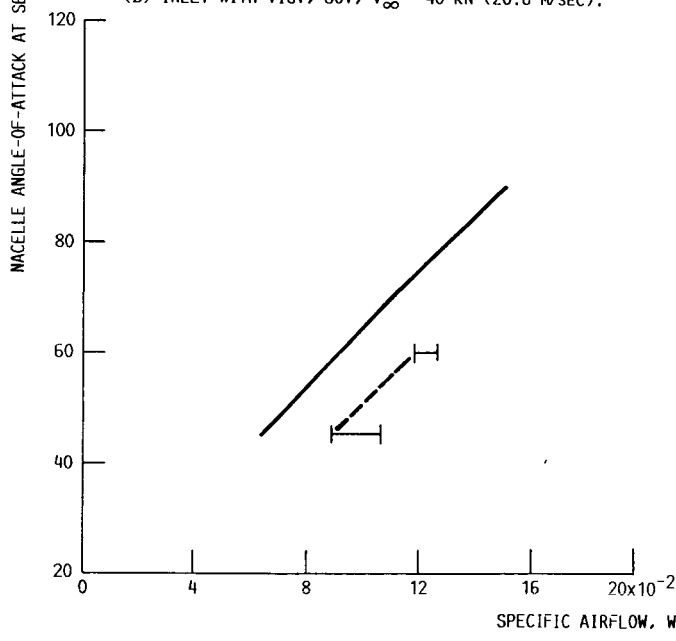
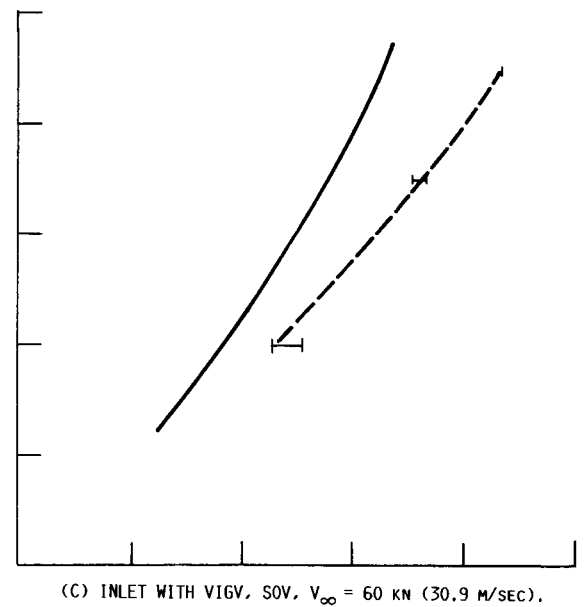
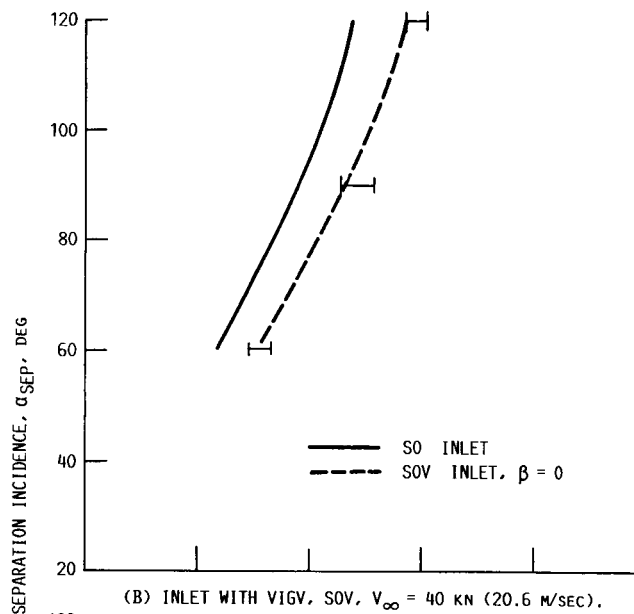


FIGURE 12. - CONCLUDED.

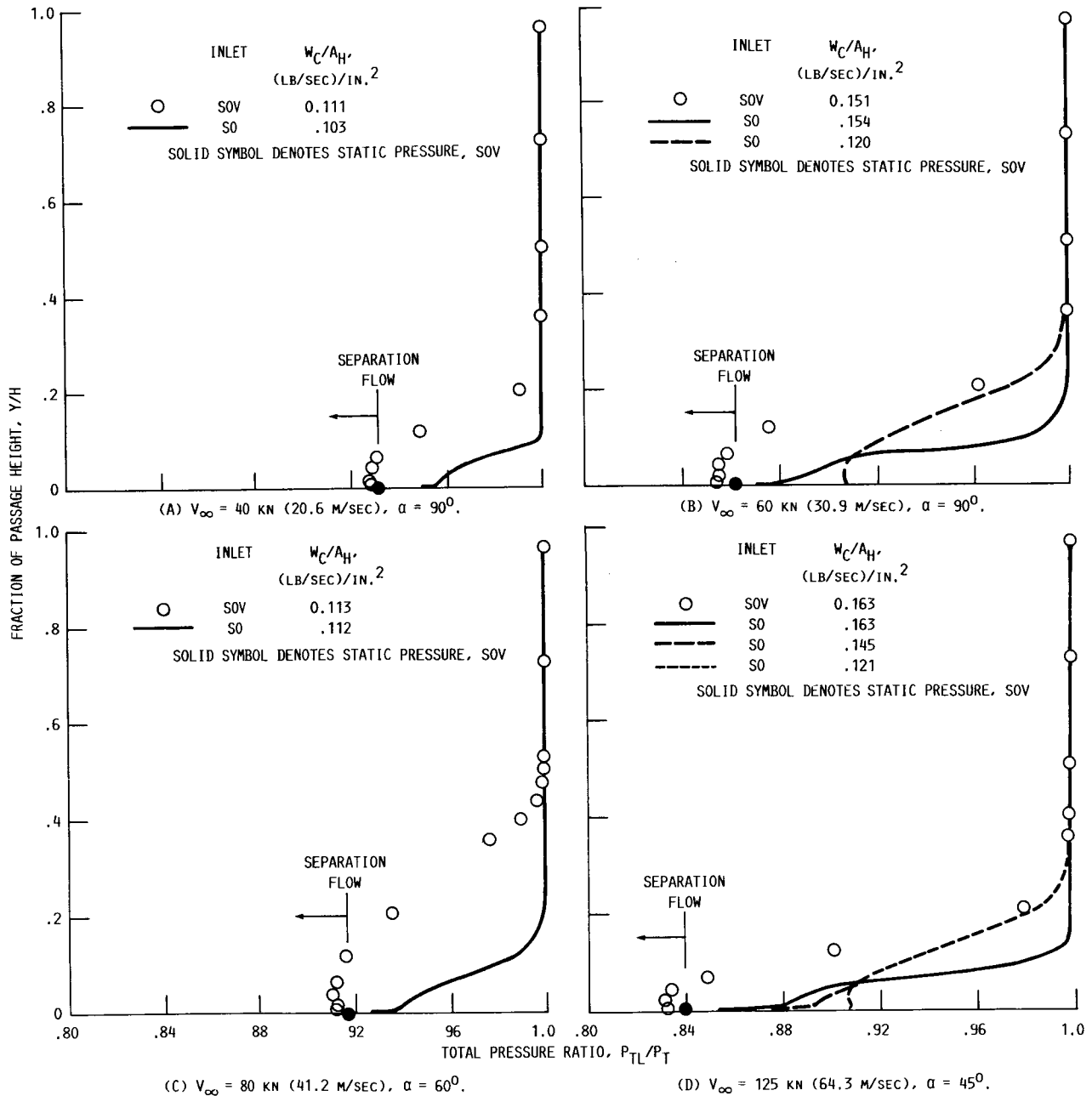
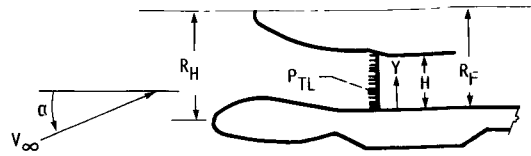


FIGURE 13. - VIGV INSTALLATION EFFECTS ON INLET DUCT EXIT BOUNDARY LAYER PROFILE WINDWARD LIP.

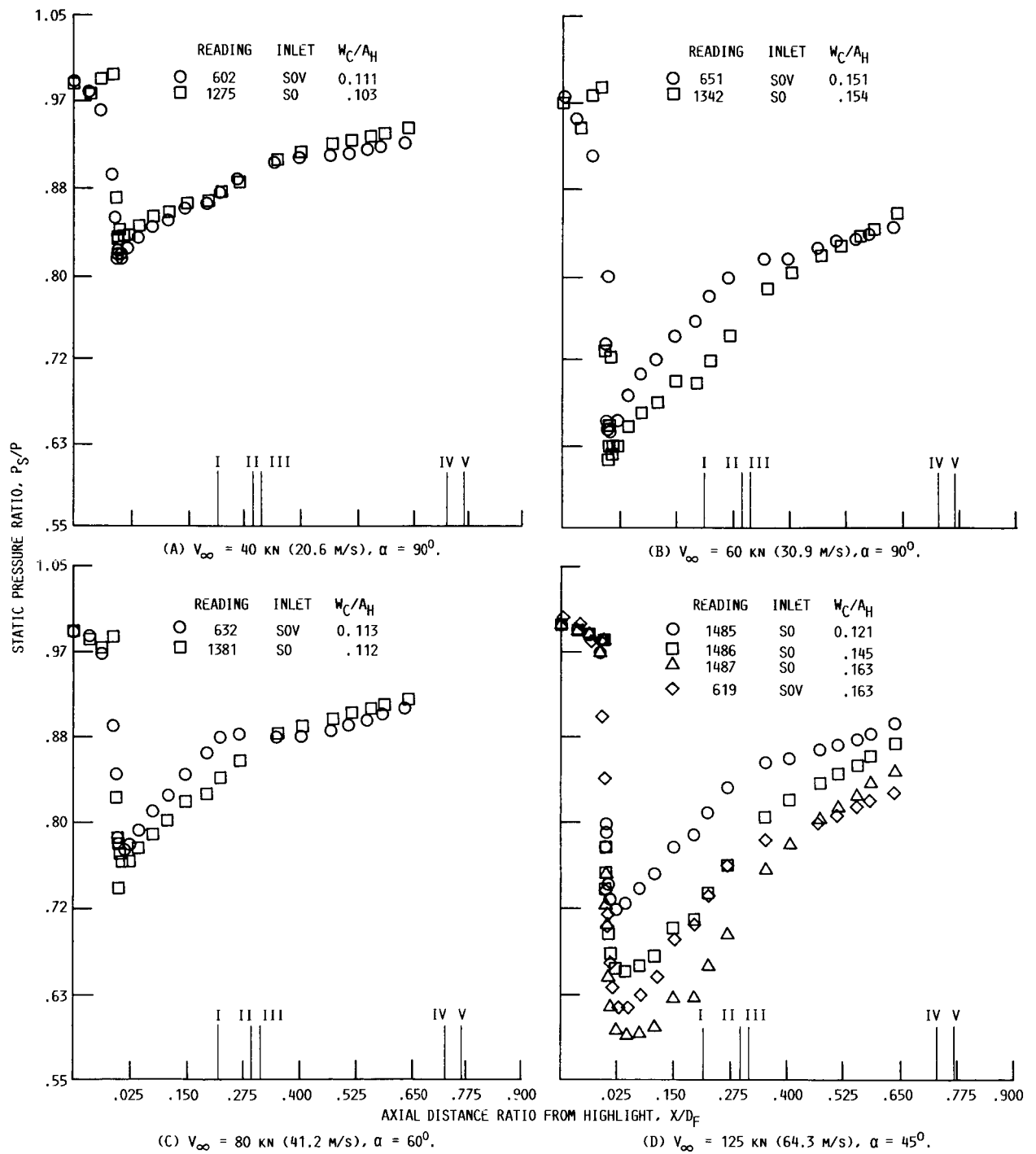


FIGURE 14. - VIGV INSTALLATION EFFECTS, DIFFUSER STATIC PRESSURE RATIO VARIATION WINDWARD LIP SIDE. AXIAL LOCATION, X/D_F , IS DENOTED BY I, 0.220 (THROAT); II, 0.290 (MIN. FLOW AREA SOV); III, 0.315 (MIN FLOW AREA SO); IV, 0.730 (FAN FACE RAKE SOV); 0.765 (FAN FACE RAKE SO).

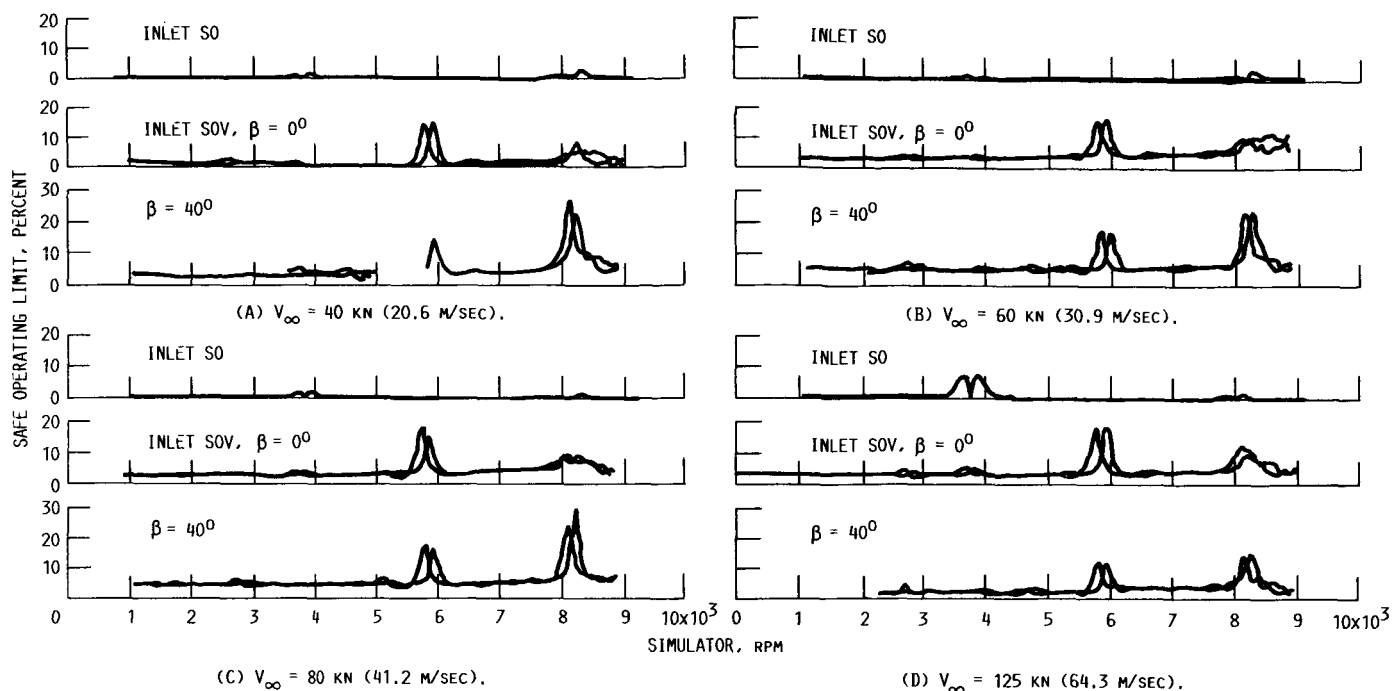


FIGURE 15. - BLADE STRESS COMPARISON AT ZERO ANGLE OF ATTACK. ENGINE ORDERS (EO) WERE 3 (8020 RPM), 4 (6015 RPM) 5 (4812 RPM), AND 6 (4010).

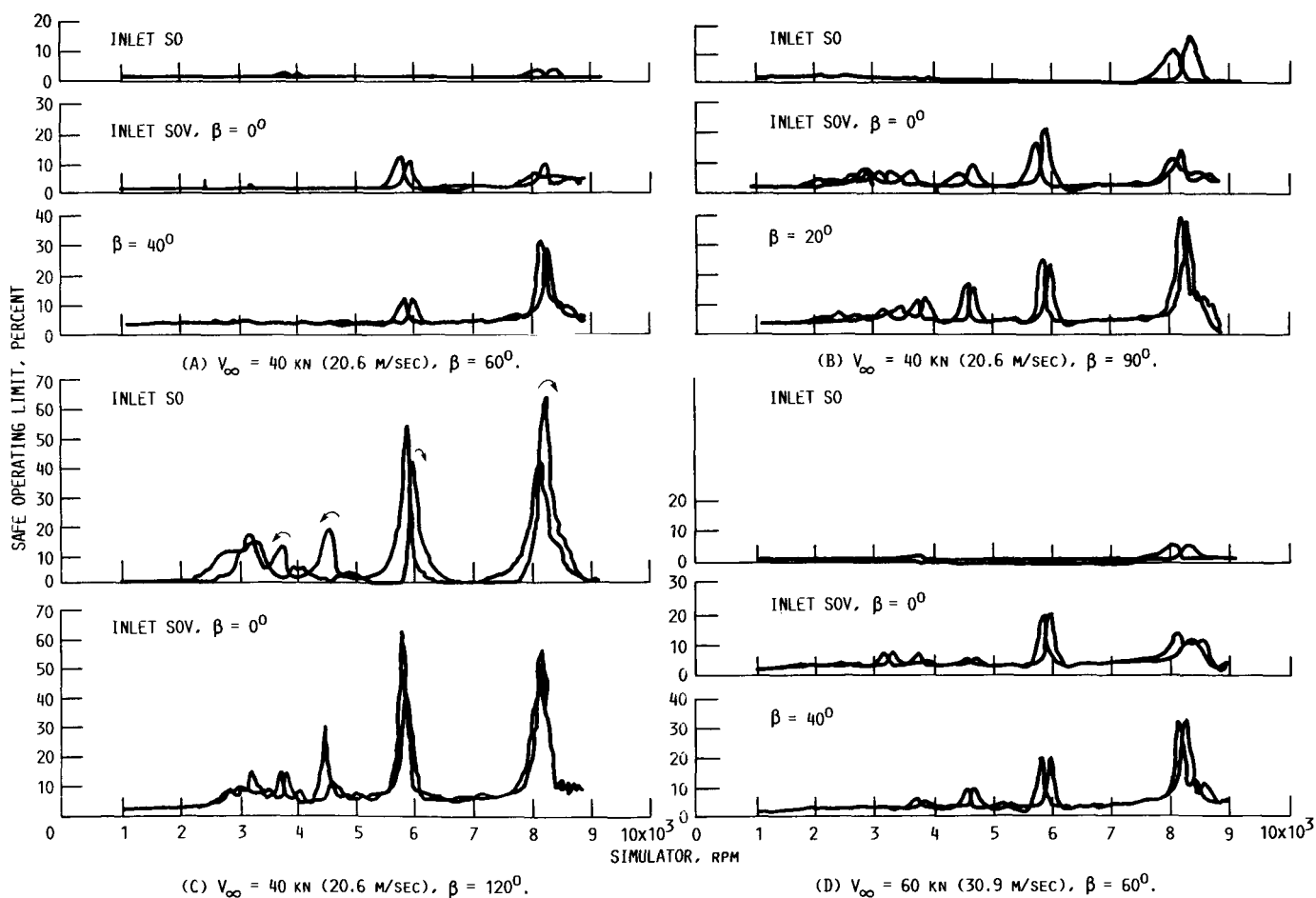


FIGURE 16. - BLADE STRESS COMPARISON AT ANGLE OF ATTACK.

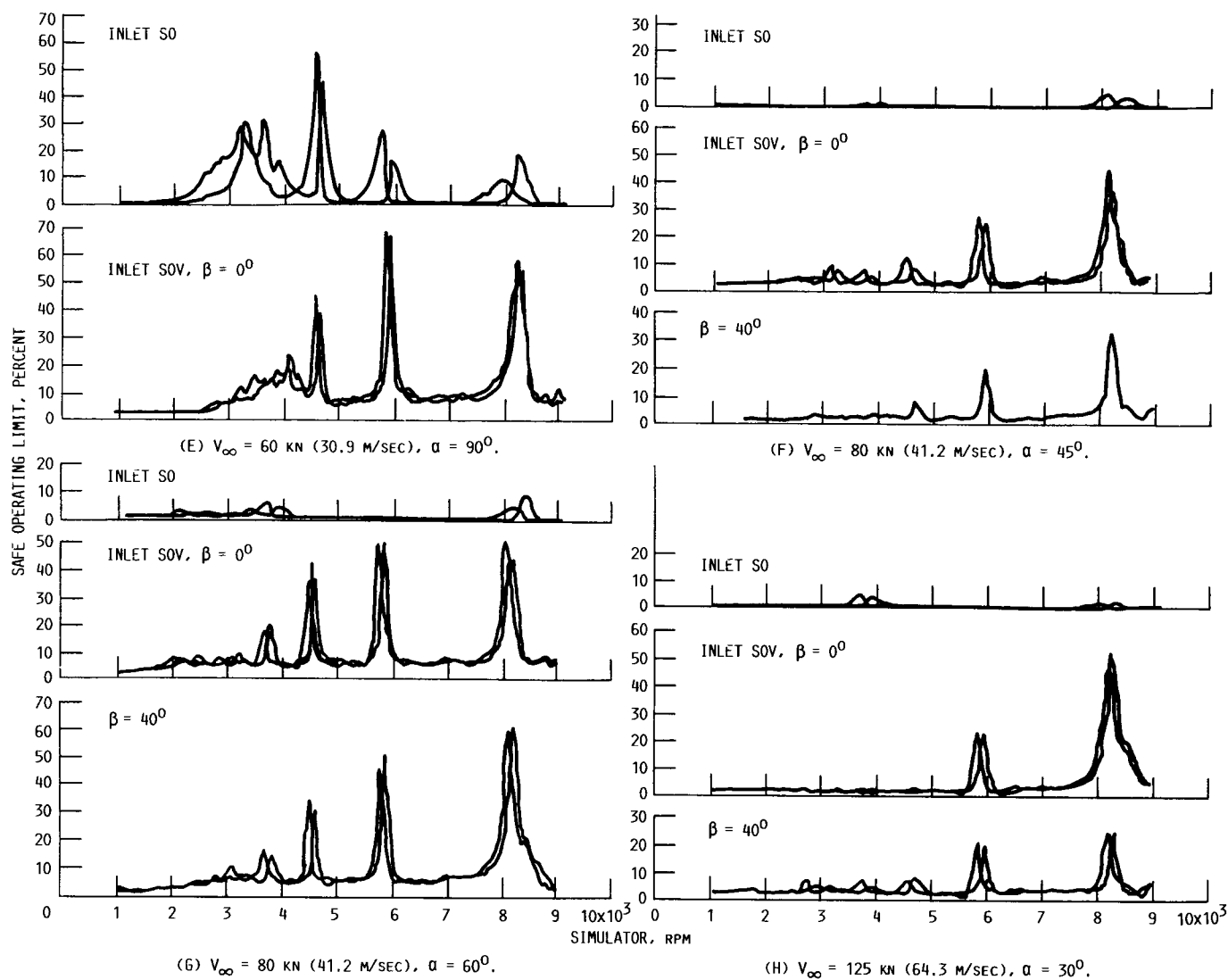


FIGURE 16. - CONTINUED.

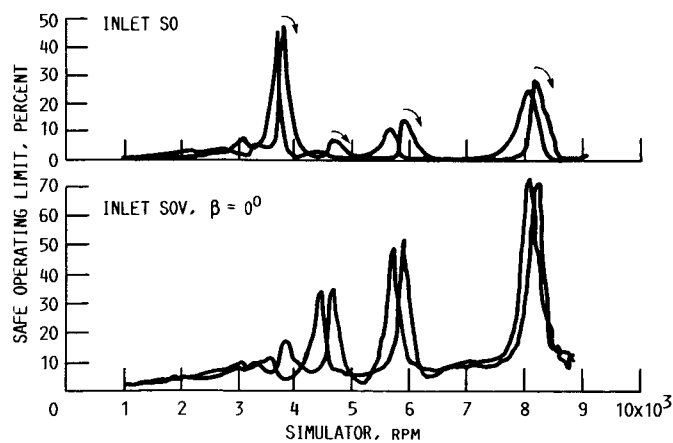


FIGURE 16. - CONCLUDED.

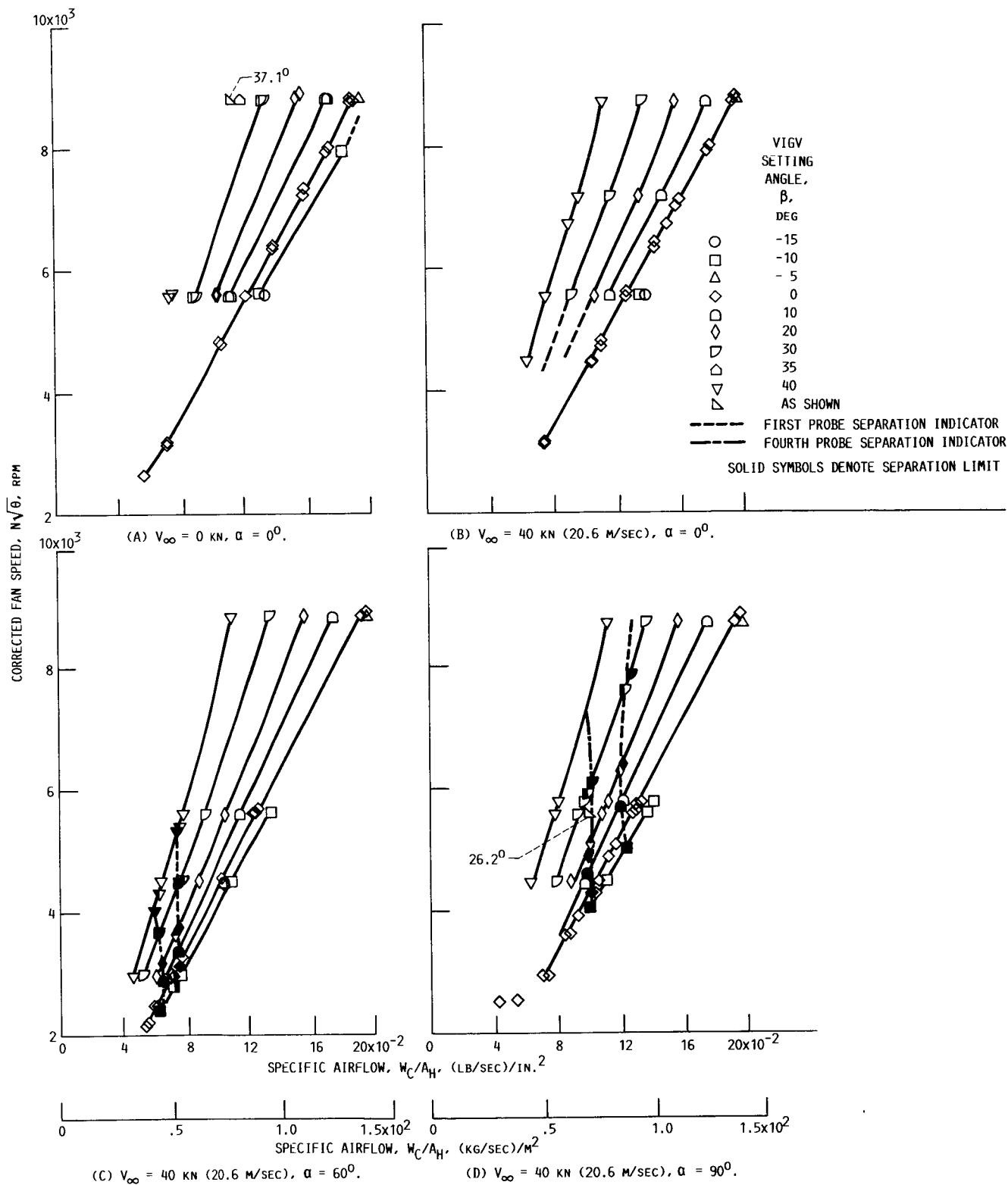


FIGURE 17. - FAN AIRFLOW CHARACTERISTICS FOR SEPARATION WITH SOV INLET.

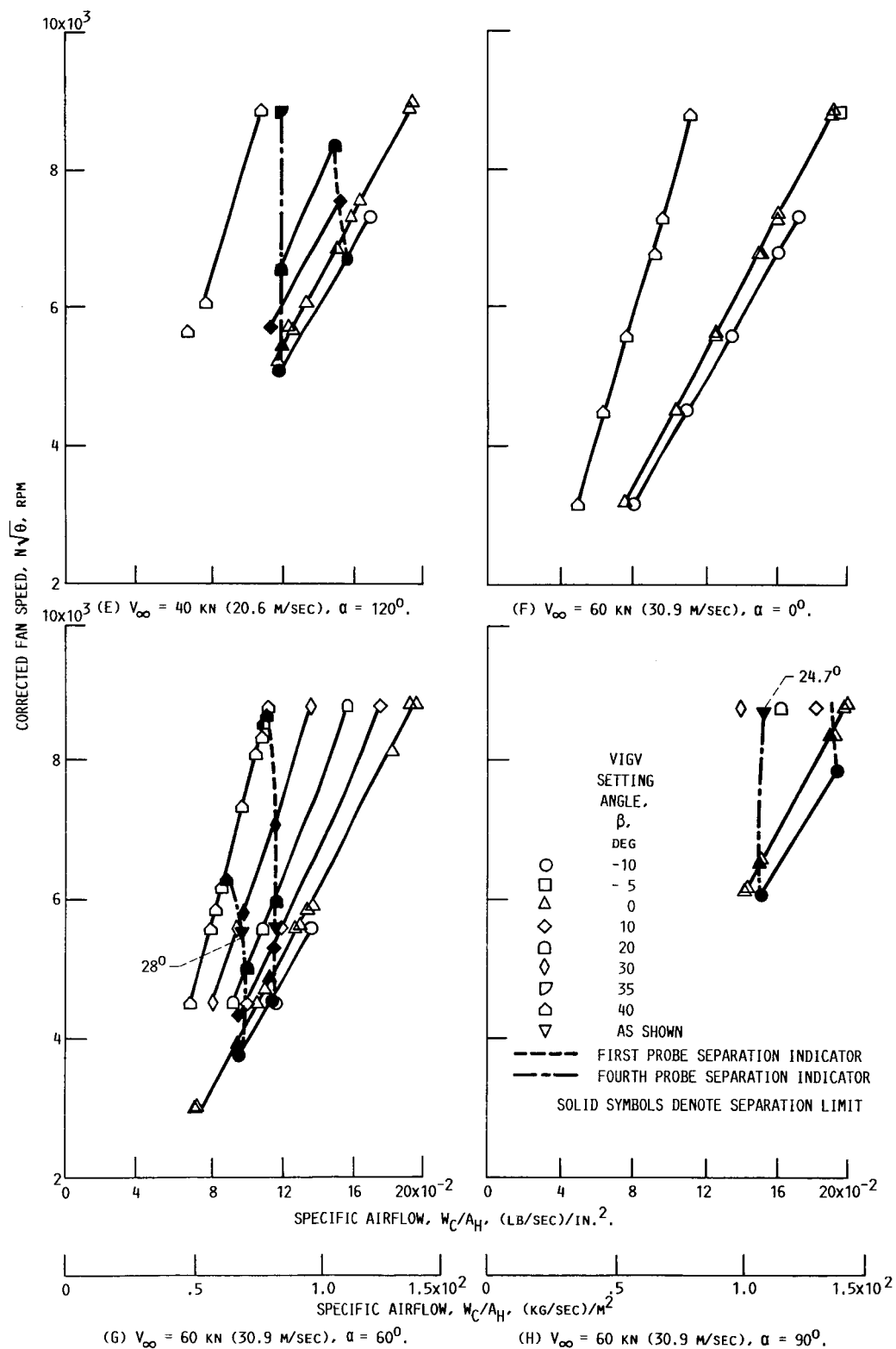


FIGURE 17. - CONTINUED.

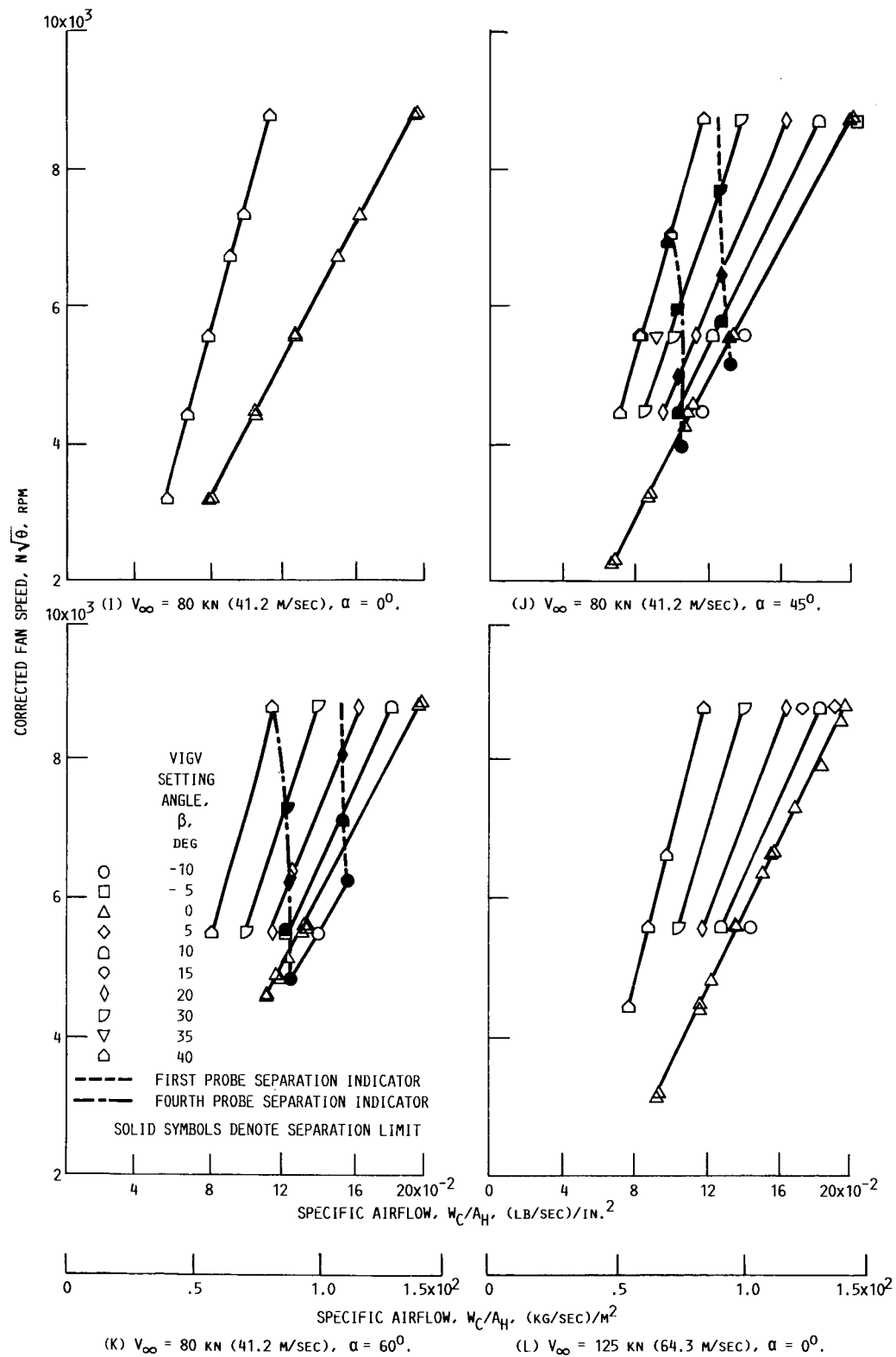
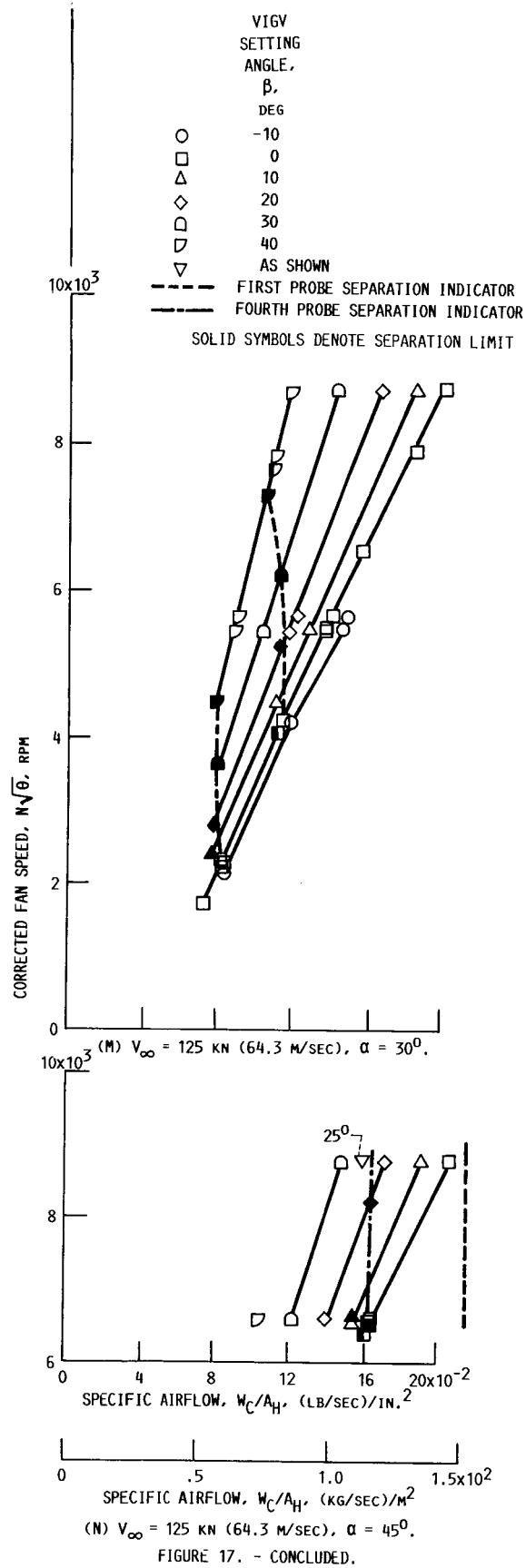
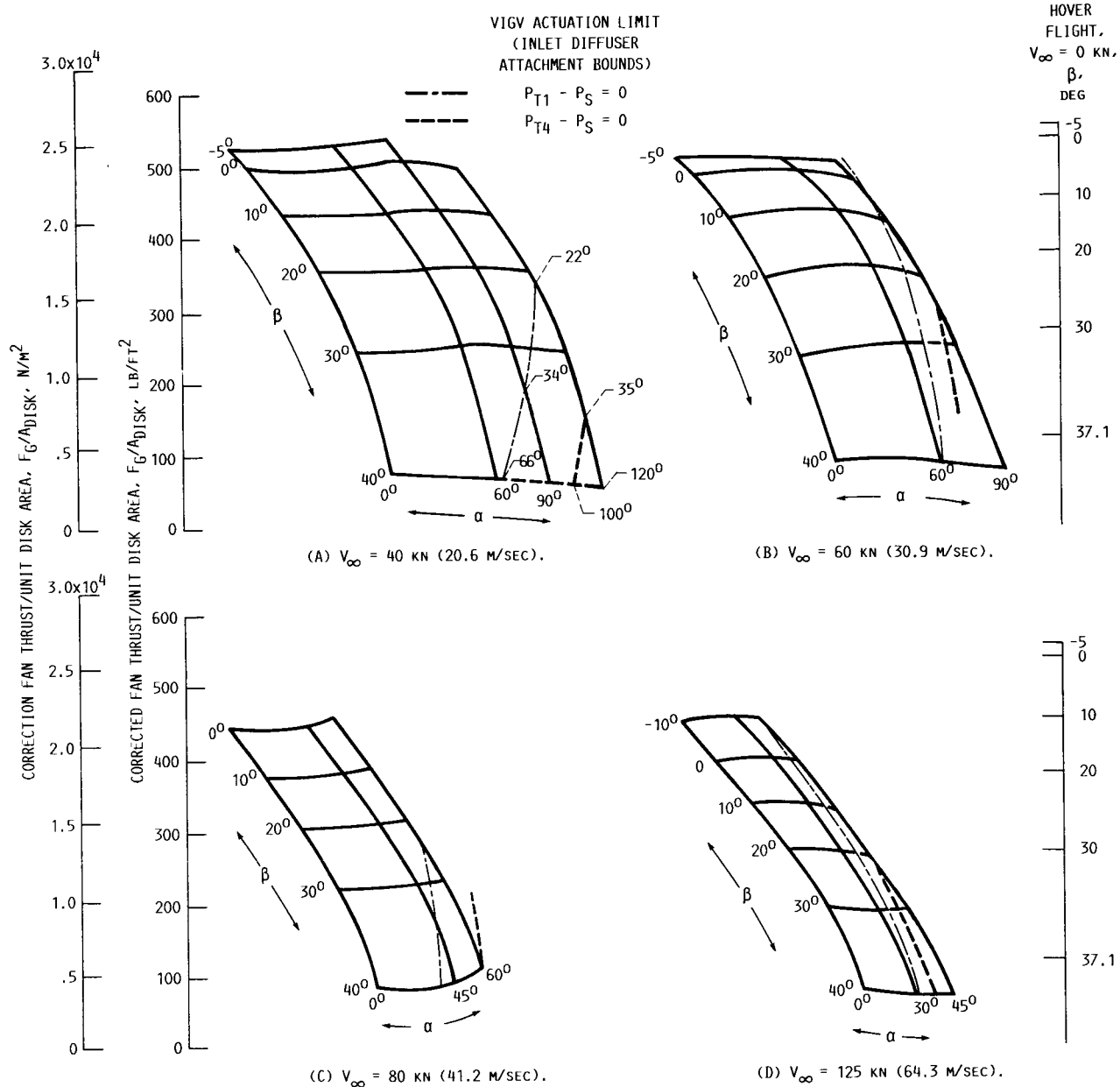


FIGURE 17. - CONTINUED.





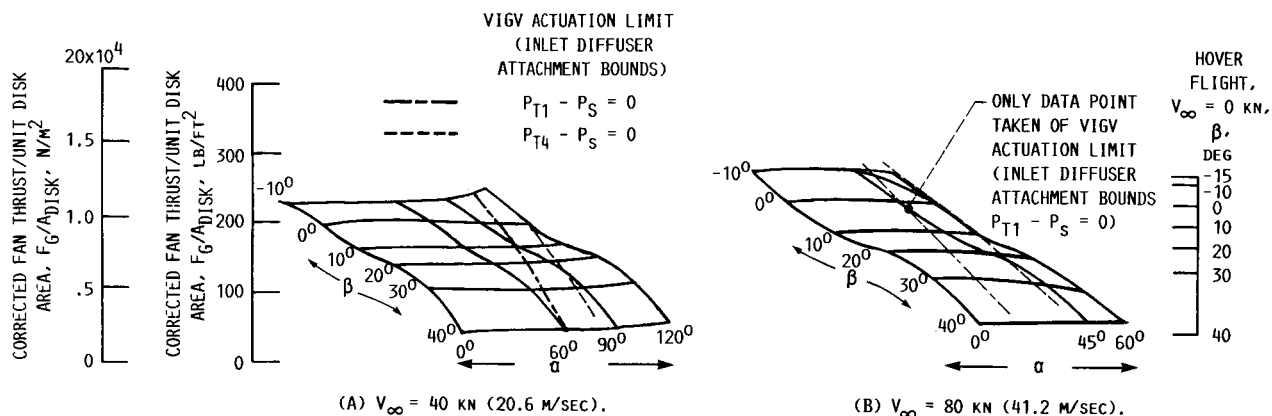


FIGURE 19. - VIGV THRUST MODULATION IN TRANSITIONAL FLIGHT, 70 PERCENT $(N/\sqrt{\theta})_{DES}$.

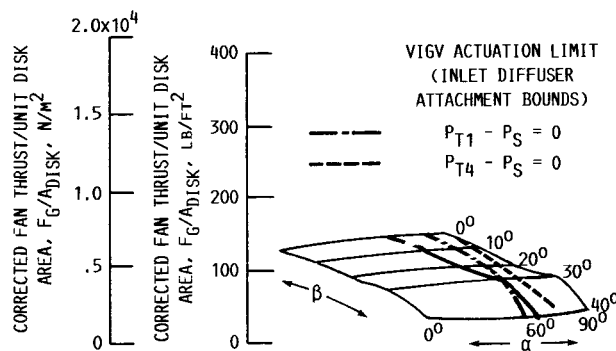


FIGURE 20. - VIGV THRUST MODULATION IN TRANSITIONAL FLIGHT, 56 PERCENT $(N/\sqrt{\theta})_{DES}$; $V_\infty = 40 \text{ kN (20.6 M/SEC)}$.

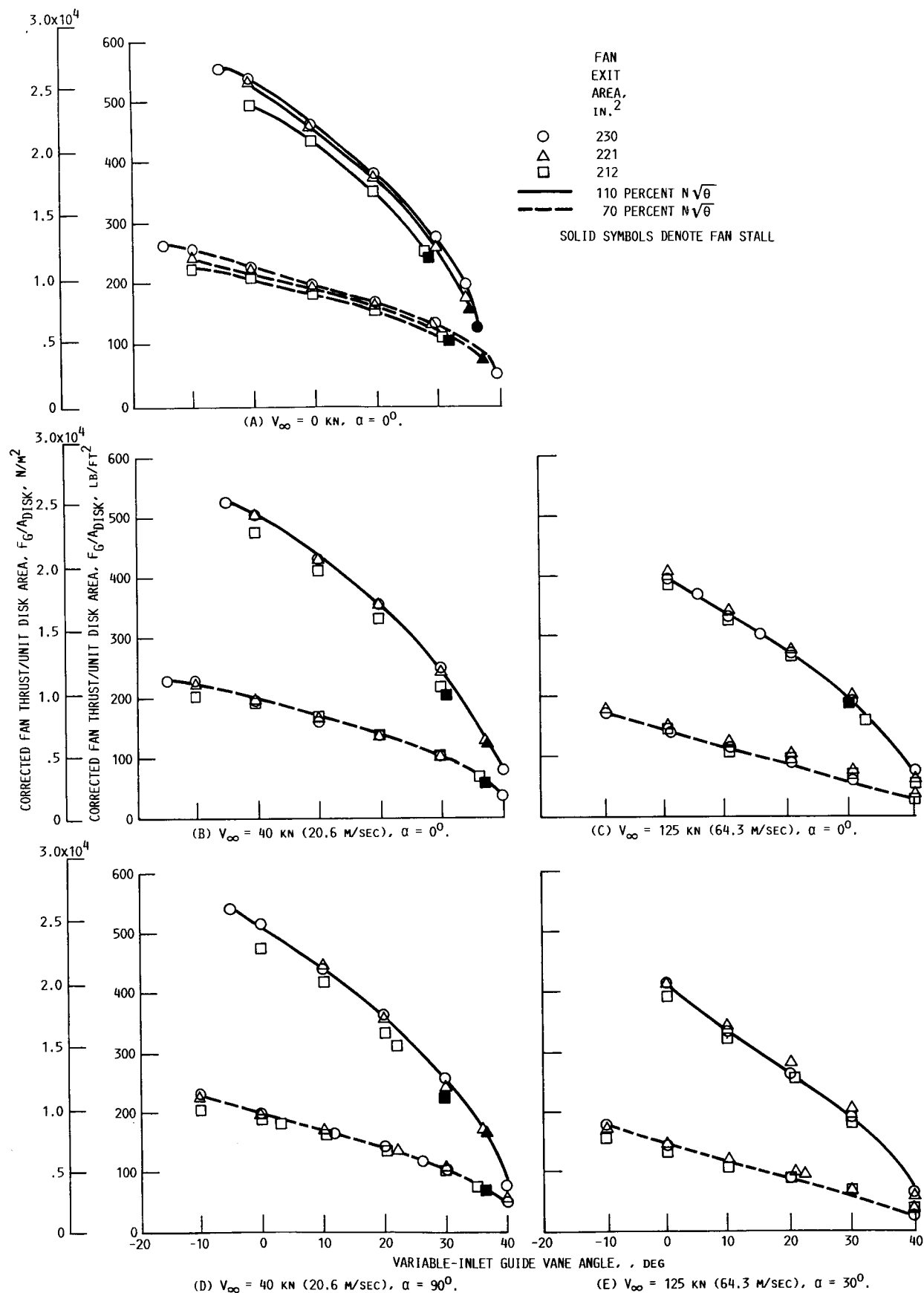


FIGURE 21. - VIGV THRUST MODULATION.

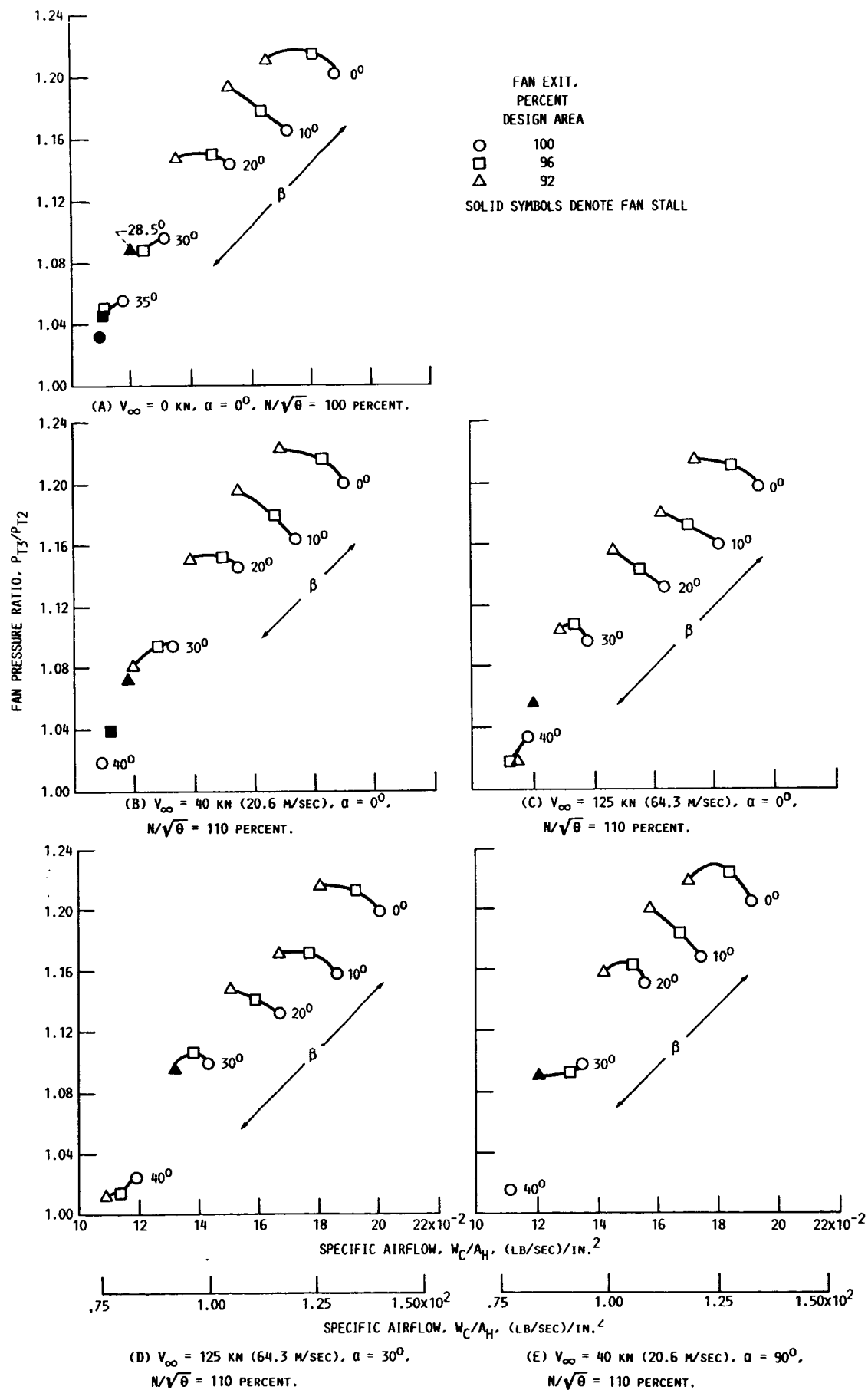


FIGURE 22. - EFFECT OF VIGV ACTUATION ON FAN STAGE PERFORMANCE.

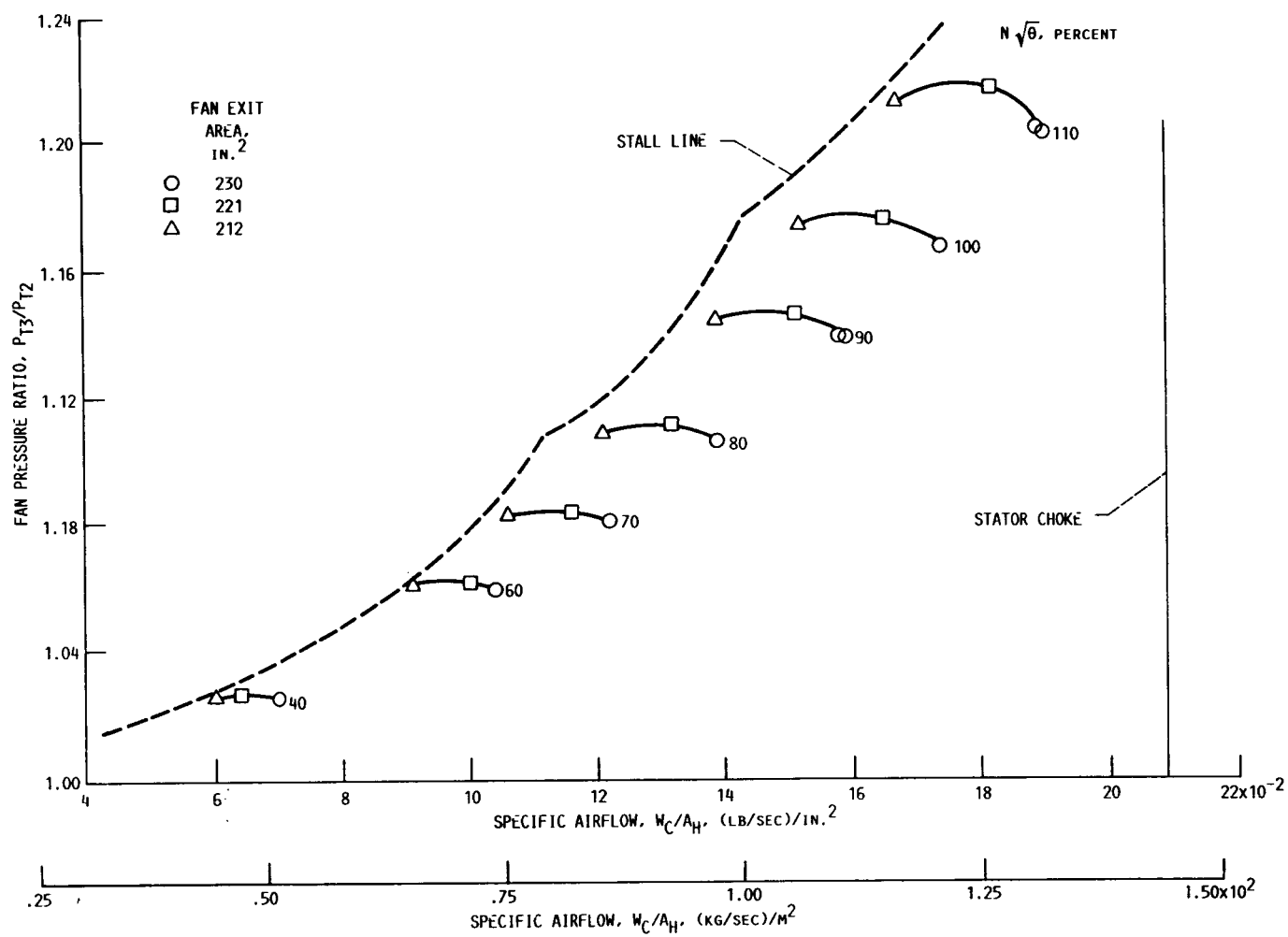


FIGURE 23. - FAN STAGE PERFORMANCE VIGV $\beta = 0^\circ$.

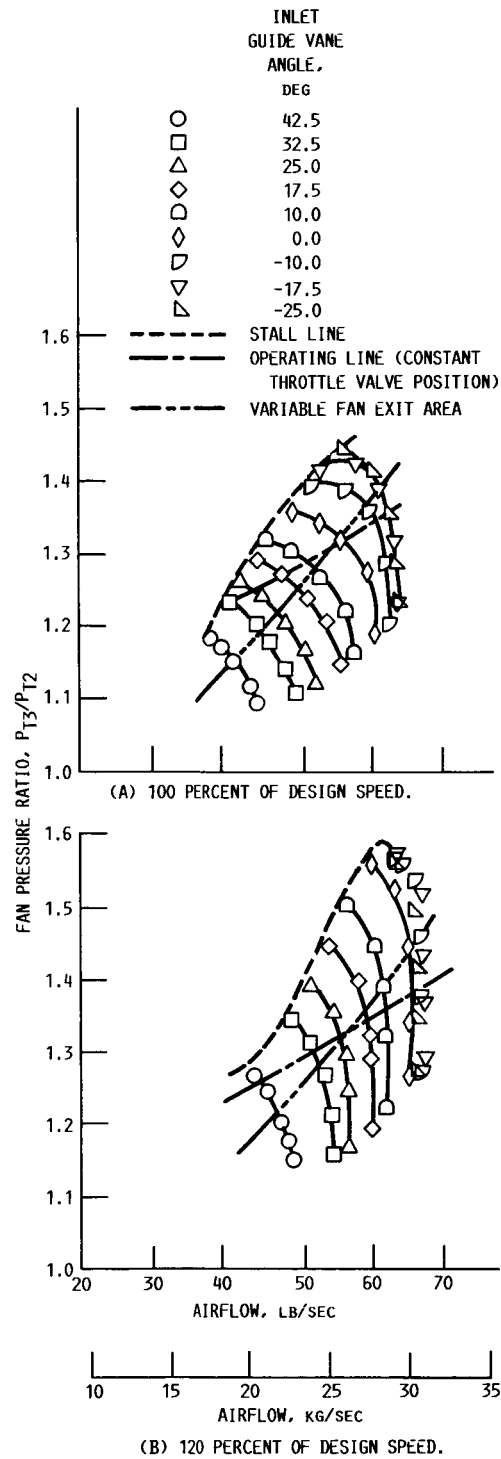


FIGURE 24. - EFFECT OF INLET GUIDE-VANE ANGLE ON OVERALL STAGE PERFORMANCE (FROM REF. 1).



National Aeronautics and
Space Administration

Report Documentation Page

1. Report No. NASA TM-88983	2. Government Accession No.	3. Recipient's Catalog No.	
4. Title and Subtitle Effect of Variable-Inlet Guide Vanes on the Operating Characteristics of a Tilt Nacelle- Inlet Powered Fan Model		5. Report Date September 1987	
		6. Performing Organization Code 505-62-91	
7. Author(s) R.R. Woollett and H.C. Pontonides		8. Performing Organization Report No. E-3453	
		10. Work Unit No.	
9. Performing Organization Name and Address National Aeronautics and Space Administration Lewis Research Center Cleveland, Ohio 44135		11. Contract or Grant No.	
		13. Type of Report and Period Covered Technical Memorandum	
12. Sponsoring Agency Name and Address National Aeronautics and Space Administration Washington, D.C. 20546		14. Sponsoring Agency Code	
15. Supplementary Notes R.R. Woollett, NASA Lewis Research Center; H.C. Pontonides, Grumman Aerospace Corporation, Bethpage, New York 11714.			
16. Abstract <p>The effects of a variable-inlet guide vane (VIGV) assembly on the operating characteristics of a V/STOL inlet and on the performance of a 20-in.- (0.508-m-) diameter fan engine were investigated. The data indicate that the VIGV's are effective thrust modulators over a wide range of free-stream velocities, nacelle angles-of-attack, and fan speeds. The thrust modulation ranges including choking limits, fan stall limits, and inlet separation boundaries are presented. The presence of the VIGV assembly causes significant losses in inlet angle-of-attack capability and generally increases the blade stress levels at all limit conditions except at high angle-of-attack and high free-stream velocity. Reducing the fan nozzle exit area limited the positive VIGV actuation range and consequently decreased the range of thrust modulation at all limit conditions except at both high free-stream velocity and high angle-of-attack conditions.</p>			
17. Key Words (Suggested by Author(s)) Inlets V/STOL Thrust modulation		18. Distribution Statement Unclassified - unlimited STAR Category 02	
19. Security Classif. (of this report) Unclassified	20. Security Classif. (of this page) Unclassified	21. No of pages 40	22. Price* A03